

METHODOLOGY ARTICLE

Open Access



A genetically encoded toolkit of functionalized nanobodies against fluorescent proteins for visualizing and manipulating intracellular signalling

David L. Prole* and Colin W. Taylor*

Abstract

Background: Intrabodies enable targeting of proteins in live cells, but generating specific intrabodies against the thousands of proteins in a proteome poses a challenge. We leverage the widespread availability of fluorescently labelled proteins to visualize and manipulate intracellular signalling pathways in live cells by using nanobodies targeting fluorescent protein tags.

Results: We generated a toolkit of plasmids encoding nanobodies against red and green fluorescent proteins (RFP and GFP variants), fused to functional modules. These include fluorescent sensors for visualization of Ca^{2+} , H^{+} and ATP/ADP dynamics; oligomerising or heterodimerising modules that allow recruitment or sequestration of proteins and identification of membrane contact sites between organelles; SNAP tags that allow labelling with fluorescent dyes and targeted chromophore-assisted light inactivation; and nanobodies targeted to luminal sub-compartments of the secretory pathway. We also developed two methods for crosslinking tagged proteins: a dimeric nanobody, and RFP-targeting and GFP-targeting nanobodies fused to complementary hetero-dimerizing domains. We show various applications of the toolkit and demonstrate, for example, that IP_3 receptors deliver Ca^{2+} to the outer membrane of only a subset of mitochondria and that only one or two sites on a mitochondrion form membrane contacts with the plasma membrane.

Conclusions: This toolkit greatly expands the utility of intrabodies and will enable a range of approaches for studying and manipulating cell signalling in live cells.

Keywords: Cell signalling, Endoplasmic reticulum, Fluorescence microscopy, Fluorescent protein, GFP, Intrabody, Membrane contact site, Mitochondria, Nanobody, RFP

Background

Visualizing the location of specific proteins within cells and manipulating their function is crucial for understanding cell biology. Antibodies can define protein locations in fixed and permeabilized cells, but antibodies are large protein complexes that are difficult to introduce into live cells [1]. This limits their ability to interrogate the dynamics or affect the function of proteins in live cells. Small protein-based binders, including nanobodies derived from the variable region of the heavy chains

(V_{HH}) of camelid antibodies, offer a promising alternative [2]. Nanobodies can be encoded by plasmids and expressed in live cells. However, generating nanobodies against thousands of protein variants is daunting, and even for single targets, it can be time-consuming, costly and not always successful. A solution to this bottleneck is provided by fluorescently tagged proteins, which are widely used in cell biology [3, 4] after heterologous expression of proteins or gene editing of endogenous proteins [5–7]. The most common application of fluorescent protein (FP) tags is to visualize protein locations, but they have additional potential as generic affinity tags

* Correspondence: dp350@cam.ac.uk; cwt1000@cam.ac.uk
Department of Pharmacology, University of Cambridge, Tennis Court Road, Cambridge CB2 1PD, UK



to manipulate and visualize protein functions in live cells. These opportunities are under-developed.

Green fluorescent protein (GFP) has undergone numerous cycles of optimization as a reporter and non-perturbing tag [3, 8]. Most GFP-tagged proteins therefore retain their endogenous localization and function [9]. Large libraries of plasmids encoding GFP-tagged proteins are now available [10]. Proteome-scale expression of GFP-tagged proteins or genome-scale tagging of gene products with GFP has been reported for *Drosophila* [11], fungi [12–14], plants [15, 16] and bacteria [17].

Proteins tagged with red fluorescent proteins (RFPs) such as DsRed, mRFP and mCherry (mCh) are also popular. Extensive optimization has made them attractive tags [3, 18], and libraries of RFP-tagged proteins have been developed in mouse stem cells [19] and yeast [14].

Nanobodies that bind to RFP [20, 21] or GFP [21, 22] are most commonly used in their purified forms for immunoprecipitation and immunocytochemistry. However, they also offer a generic means of targeting in live cells the huge variety of available tagged proteins and the many emerging examples of endogenous proteins tagged with FPs by gene editing. GFP-targeting nanobodies have been used for applications such as targeted proteasomal degradation [23, 24] and relocation of proteins in cells [25], but these and other applications are less developed for RFP-targeting nanobodies.

Here we develop a plasmid-encoded toolkit of nanobodies that bind common FP tags, including RFPs, CFP, GFP and YFP, fused to functional modules for visualization and manipulation of cell signalling (Fig. 1). We fused the nanobodies to a variety of functional modules: fluorescent sensors for Ca^{2+} , H^+ and ATP/ADP; optimized SNAP tags for labelling with bright and photostable dyes [26]; and hetero-dimerizing partners that allow inducible recruitment or sequestration of proteins and visualization of membrane contact sites (MCS) between organelles. We developed two methods to allow crosslinking of RFP-tagged and GFP-tagged proteins: a dimeric nanobody, and co-expression of RFP-targeting and GFP-targeting nanobodies fused to complementary hetero-dimerizing domains. We also describe functionalized nanobodies directed to luminal sub-compartments of the secretory pathway. We demonstrate the utility of nanobody fusions by visualizing local Ca^{2+} dynamics at the surface of mitochondria, by manipulating the locations of proteins and organelles within cells, by characterizing MCS between mitochondria and the plasma membrane (PM) and by targeting luminal Ca^{2+} sensors to a sub-compartment of the endoplasmic reticulum (ER).

This versatile toolkit of genetically encoded, functionalized nanobodies greatly expands the utility of RFP- and GFP-targeting nanobodies. It will provide a valuable resource for studying protein function and cell signalling in live cells. We illustrate some applications and demonstrate,

for example, that IP_3 receptors deliver Ca^{2+} to the outer membrane of only some mitochondria and that MCS between mitochondria and the plasma membrane occur at only one or two sites on each mitochondrion.

Results

Targeting RFP and GFP variants with genetically encoded nanobody fusions in live cells

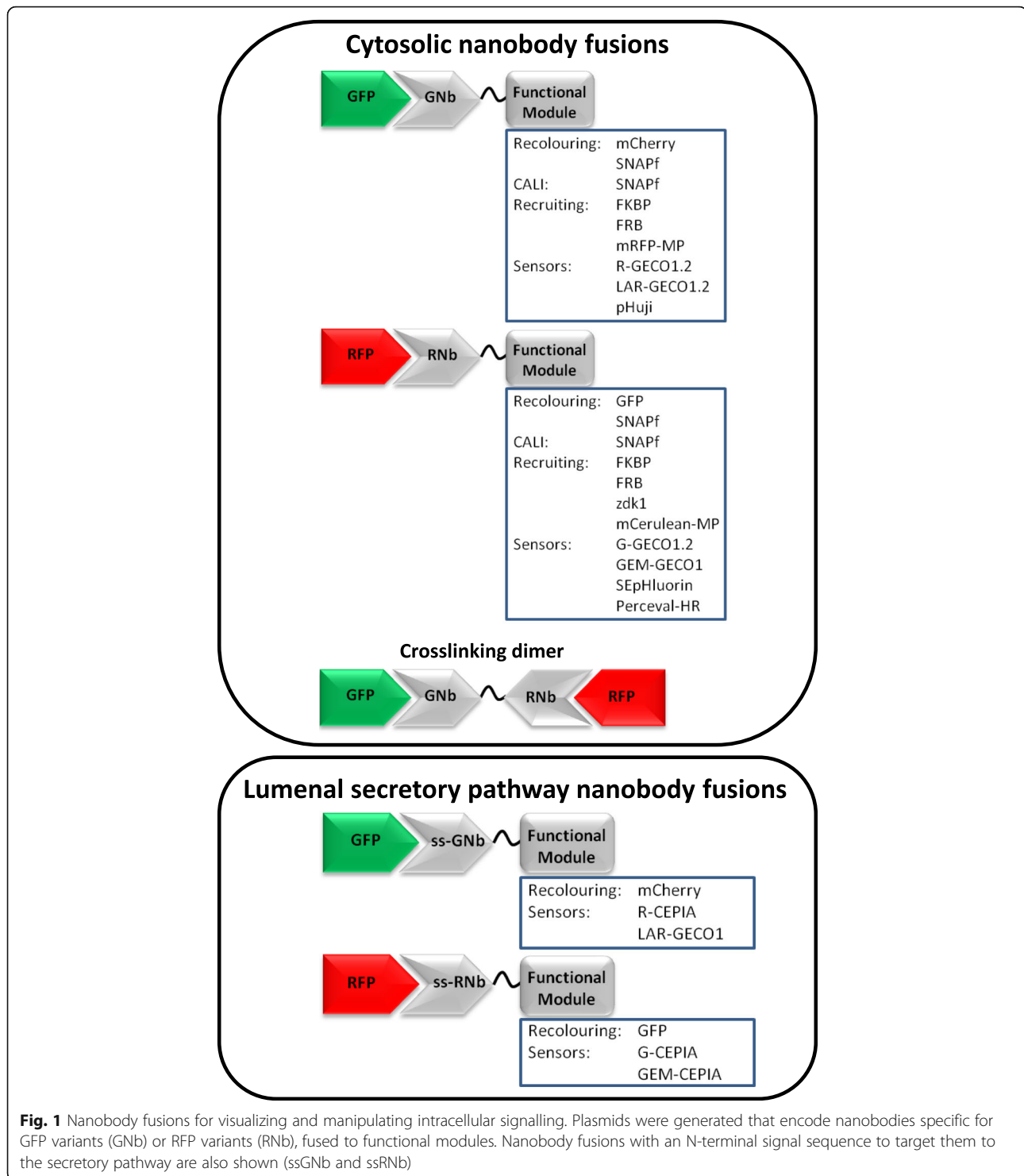
The RFP nanobody (RNb) and GFP nanobody (GNb) used are the previously described llama variants LaM4 and LaG16, respectively [21]. They were chosen for their favourable combinations of high affinity (K_d values of 0.18 nM and 0.69 nM, respectively) and the ability to bind a variety of RFP or GFP variants [21]. The latter attribute maximizes their potential for targeting a wide variety of FPs [3, 4]. LaM4 binds both mCh and DsRed variants, but not GFPs [21]. In addition to binding GFP, LaG16 binds cyan, blue and yellow FPs (CFP, BFP and YFP), but not RFPs [21]. In contrast, the widely used VhhGFP4 nanobody binds GFP, but not CFP [22].

In HeLa cells with organelles (ER, mitochondria, nucleus and lysosomes) labelled with mCh or mRFP markers, expression of RNb-GFP (Fig. 2a) specifically identified the labelled organelle (Fig. 2b). Similar results were obtained with GNb-mCh (Fig. 2c) and organelles (ER, mitochondria and nucleus) labelled with GFP or mTurquoise (Fig. 2d). These results demonstrate that plasmid-encoded RNb and GNb allow specific labelling of a variety of RFP and GFP variants in live cells.

Targeting sensors to RFP and GFP

The effects of intracellular messengers such as Ca^{2+} [27], H^+ [28] and ATP/ADP [29] can be highly localized within cells. To enable visualization of these intracellular messengers in microdomains around RFP-tagged and GFP-tagged proteins, we fused RNb and GNb to fluorescent sensors for Ca^{2+} [30], H^+ [31, 32] or ATP/ADP [33].

RNb was fused to the green fluorescent Ca^{2+} sensor G-GECO1.2 (Fig. 3), and GNb was fused to the red fluorescent Ca^{2+} sensors, R-GECO1.2 or LAR-GECO1.2 [30] (Fig. 4). The affinities of these sensors for Ca^{2+} (K_D^{Ca} of 1.2 μM for G-GECO1.2 and R-GECO1.2, and 10 μM for LAR-GECO1.2) are low relative to global changes in the cytosolic free Ca^{2+} concentration ($[\text{Ca}^{2+}]_c$) after receptor stimulation (typically ~ 300 nM) [34]. This facilitates selective detection of the large, local rises in $[\text{Ca}^{2+}]$ that are important for intracellular signalling, at the contacts between active inositol 1,4,5-trisphosphate receptors (IP_3Rs) and mitochondria, for example [27]. To allow targeted measurement of relatively low resting $[\text{Ca}^{2+}]$ within cellular microdomains, we also fused RNb to the ratiometric Ca^{2+} -sensor, GEMGECO1 ($K_D^{\text{Ca}} = 300$ nM) [30], to give RNb-GEMGECO1 (Additional file 1: Figure S1).



In HeLa cells expressing TOM20-mCh or TOM20-GFP to identify the outer mitochondrial membrane (OMM), the RNb- Ca^{2+} sensors (Fig. 3 and Additional file 1: Figure S1) and GNb- Ca^{2+} sensors (Fig. 4) were targeted to the OMM. Both families of targeted sensor reported an increase in $[\text{Ca}^{2+}]_c$ after treatment with the Ca^{2+} ionophore,

ionomycin (Figs. 3 and 4 and Additional file 1: Figure S1). This confirms the ability of the sensors to report $[\text{Ca}^{2+}]_c$ changes when targeted to the OMM microdomain.

In some cells, the targeted Nb- Ca^{2+} sensors revealed local changes in $[\text{Ca}^{2+}]_c$ after receptor stimulation with histamine, which stimulates IP_3 formation and Ca^{2+}

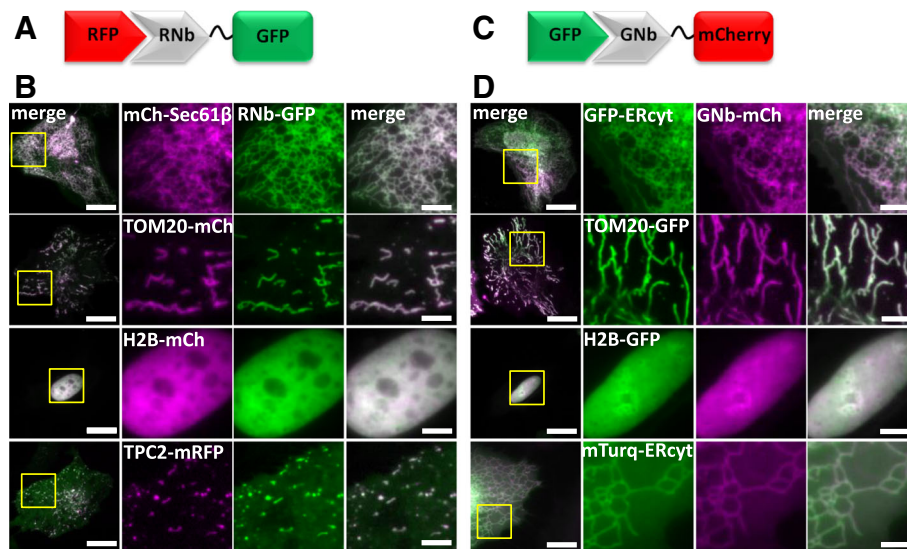


Fig. 2 RNb and GNb fusion proteins bind to their respective tagged proteins in live cells. **a** Schematic of the RNb-GFP fusion binding to RFP. **b** HeLa cells expressing RNb-GFP with RFP-tagged markers for the ER surface (mCh-Sec61 β), the mitochondrial surface (TOM20-mCh), the nucleus (H2B-mCh), or the surface of lysosomes (TPC2-mRFP). Cells were imaged in HBS using epifluorescence microscopy (cells expressing H2B-mCh) or TIRFM (other cells). Yellow boxes indicate regions enlarged in the subsequent panels. Colocalization values (Pearson's coefficient, r) were mCh-Sec61 β ($r = 0.93 \pm 0.09$, $n = 10$ cells), TOM20-mCh ($r = 0.94 \pm 0.09$, $n = 10$ cells), H2B-mCh ($r = 0.97 \pm 0.06$, $n = 10$ cells), and TPC2-mRFP ($r = 0.78 \pm 0.09$, $n = 5$ cells). **c** Schematic of the GNb-mCh fusion binding to GFP. **d** HeLa cells co-expressing GNb-mCh with GFP-tagged markers for the ER surface (GFP-ERcyt), the mitochondrial surface (TOM20-GFP), and the nucleus (H2B-GFP), or an mTurquoise2-tagged ER surface marker (mTurq-ERcyt). Cells were imaged using epifluorescence microscopy (cells expressing H2B-GFP) or TIRFM (other cells). Yellow boxes indicate regions enlarged in the subsequent panels. Colocalization values were GFP-ERcyt ($r = 0.92 \pm 0.08$, $n = 8$ cells), TOM20-GFP ($r = 0.87 \pm 0.05$, $n = 7$ cells), H2B-GFP ($r = 0.94 \pm 0.07$, $n = 6$ cells), and mTurq-ERcyt ($r = 0.97 \pm 0.03$, $n = 7$ cells). Scale bars 10 μ m (main images) or 2.5 μ m (enlargements)

release from the ER in HeLa cells [34]. Imperfect targeting of the RNb-GGECO1.2 to the OMM allowed Ca^{2+} signals at the surface of individual mitochondria to be distinguished from those in nearby cytosol in some cells (Fig. 3d–f and Additional file 2: Video 1). In the example shown, RNb-GGECO1.2 at both the OMM and nearby cytosol responded to the large, global increases in $[\text{Ca}^{2+}]$ evoked by ionomycin. However, cytosolic RNb-GGECO1.2 did not respond to histamine, while the sensor at the OMM responded with repetitive spiking (Fig. 3d–f and Additional file 2: Video 1). The GNb-LARGECO1.2 sensor, which has the lowest affinity for Ca^{2+} of the sensors used, revealed changes in $[\text{Ca}^{2+}]_c$ at the surface of some mitochondria, but not others in the same cell (Fig. 4d–f, Fig. 4h and Additional file 3: Video 2). In the example shown, GNb-LARGECO1.2 at the OMM in all mitochondria within the cell responded to the large, global increases in $[\text{Ca}^{2+}]$ evoked by ionomycin. However, in response to histamine, mitochondria in the perinuclear region responded, but not those in peripheral regions (Fig. 4d–f, Fig. 4h and Additional file 3: Video 2). Ca^{2+} uptake by mitochondria affects many cellular responses, including mitochondrial metabolism, ATP production and apoptosis [35]; and Ca^{2+} at the cytosolic face of the OMM regulates mitochondrial motility [36]. The subcellular heterogeneity

of mitochondrial exposure to increased $[\text{Ca}^{2+}]$ suggests that these responses may be very localized in cells.

These observations align with previous reports showing that Ca^{2+} -mobilizing receptors evoke both oscillatory $[\text{Ca}^{2+}]$ changes within the mitochondrial matrix [37], and large local increases in $[\text{Ca}^{2+}]$ at the cytosolic face of the OMM [38]. Our results establish that nanobody- Ca^{2+} -sensor fusions are functional and appropriately targeted and can be used to detect physiological changes in $[\text{Ca}^{2+}]$ within cellular microdomains such as the OMM.

For targeted measurements of intracellular pH, RNb was fused to the green fluorescent pH sensor super-ecliptic pHluorin (SEpHluorin) [31], and GNb was fused to the red fluorescent pH sensor pHuji [32]. Both Nb-pH sensors were targeted to the OMM by the appropriate fluorescent tags, where they responded to changes in intracellular pH imposed by altering extracellular pH in the presence of the H^+/K^+ ionophore nigericin (Fig. 5).

For targeted measurements of ATP/ADP, RNb was fused to the excitation-ratiometric ATP/ADP sensor Perceval-HR [33]. RNb-Perceval-HR was targeted to the surface of mitochondria and responded to inhibition of glycolysis and oxidative phosphorylation (Fig. 6).

The results demonstrate that nanobodies can be used to direct sensors for Ca^{2+} , H^+ or ATP/ADP to

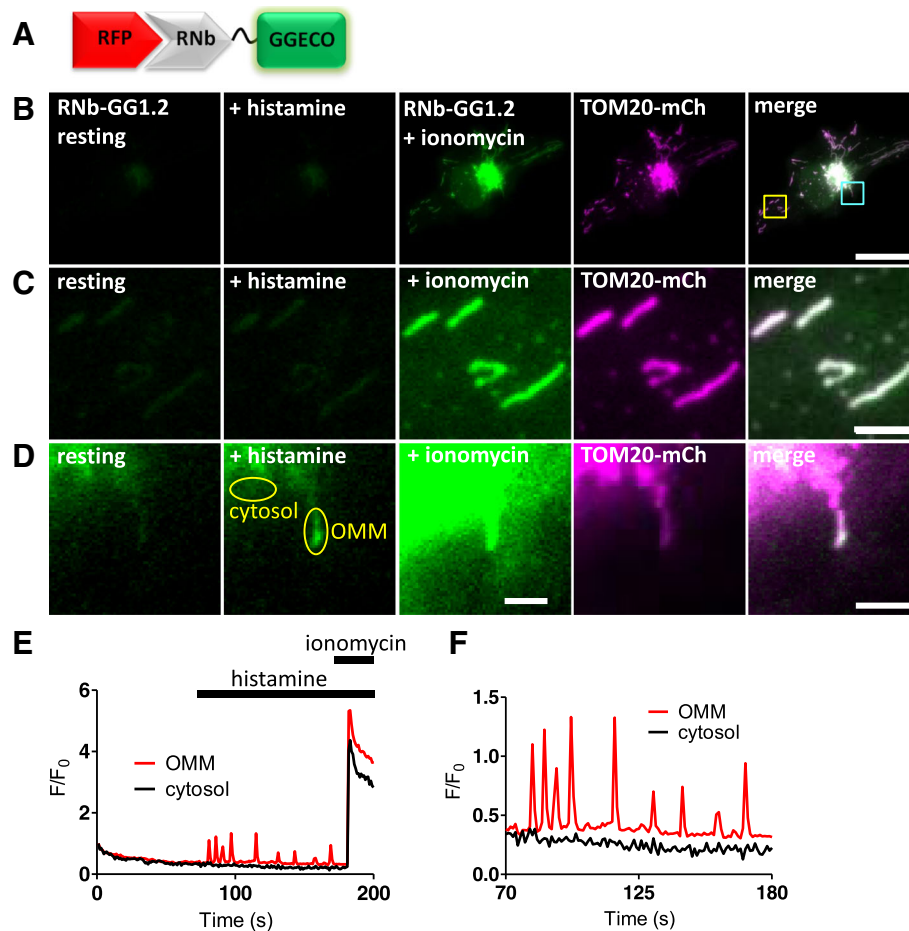


Fig. 3 Targeting RNB- Ca^{2+} sensors to RFP-tagged proteins. **a** Schematic of RNB-GGECO fusion binding to RFP. **b–d** HeLa cells expressing RNB-GGECO1.2 and TOM20-mCh, before and after addition of histamine (100 μ M) and then ionomycin (5 μ M). Cells were imaged in HBS using TIRFM. The TOM20-mCh image is shown after the histamine and ionomycin additions. The merged images are shown using images of RNB-GGECO1.2 after ionomycin (**b**, **c**) or histamine (**d**). The yellow and cyan-boxed regions in panel **b** are shown enlarged in panels **c** and **d**, respectively. Scale bars are 10 μ m (**b**) or 1.25 μ m (**c**, **d**). **e** Timecourse of the effects of histamine (100 μ M) and ionomycin (5 μ M) on the fluorescence of RNB-GGECO1.2 (F/F_0), where F and F_0 are fluorescence recorded at t and $t=0$. The traces are from regions coinciding with a single mitochondrion or cytosol (regions identified in panel **d**), indicating changes in $[\text{Ca}^{2+}]$ at the OMM. **f** Enlarged region (70–180 s) of the graph is shown in **e**. Results are representative of cells from 13 independent experiments

specific subcellular compartments tagged with variants of RFP or GFP.

Targeting SNAPf tags to RFP and GFP in live cells

SNAP, and related tags, are versatile because a range of SNAP substrates, including some that are membrane-permeant, can be used to attach different fluorophores or cargoes to the tag [39]. Purified GFP-targeting nanobodies fused to a SNAP-tag have been used to label fixed cells for optically demanding applications [40]. We extended this strategy to live cells using RNB and GNB fused to the optimized SNAPf tag [41] (Fig. 7a, b). In cells expressing the mitochondrial marker TOM20-mCh, RNB-SNAPf enabled labelling of mitochondria with the cell-permeable substrate SNAP-Cell 647-SiR and imaging at far-red

wavelengths (Fig. 7c). In cells expressing lysosomal LAMP1-mCh and RNB-SNAPf, SNAP-Cell 647-SiR instead labelled lysosomes (Fig. 7d), demonstrating that SNAP-Cell 647-SiR specifically labelled the organelles targeted by RNB-SNAPf. Similar targeting of SNAP-Cell 647-SiR to mitochondria (Fig. 7e) and lysosomes (Fig. 7f) was achieved by GNB-SNAPf co-expressed with the appropriate GFP-tagged organelle markers.

Chromophore-assisted light inactivation (CALI) can inactivate proteins or organelles by exciting fluorophores attached to them that locally generate damaging reactive superoxide. Historically, antibodies were used to direct a photosensitizer to its target, but the fusion of fluorescent proteins or SNAP-tags to proteins of interest is now widely used [42]. RNB-SNAPf and GNB-SNAPf make

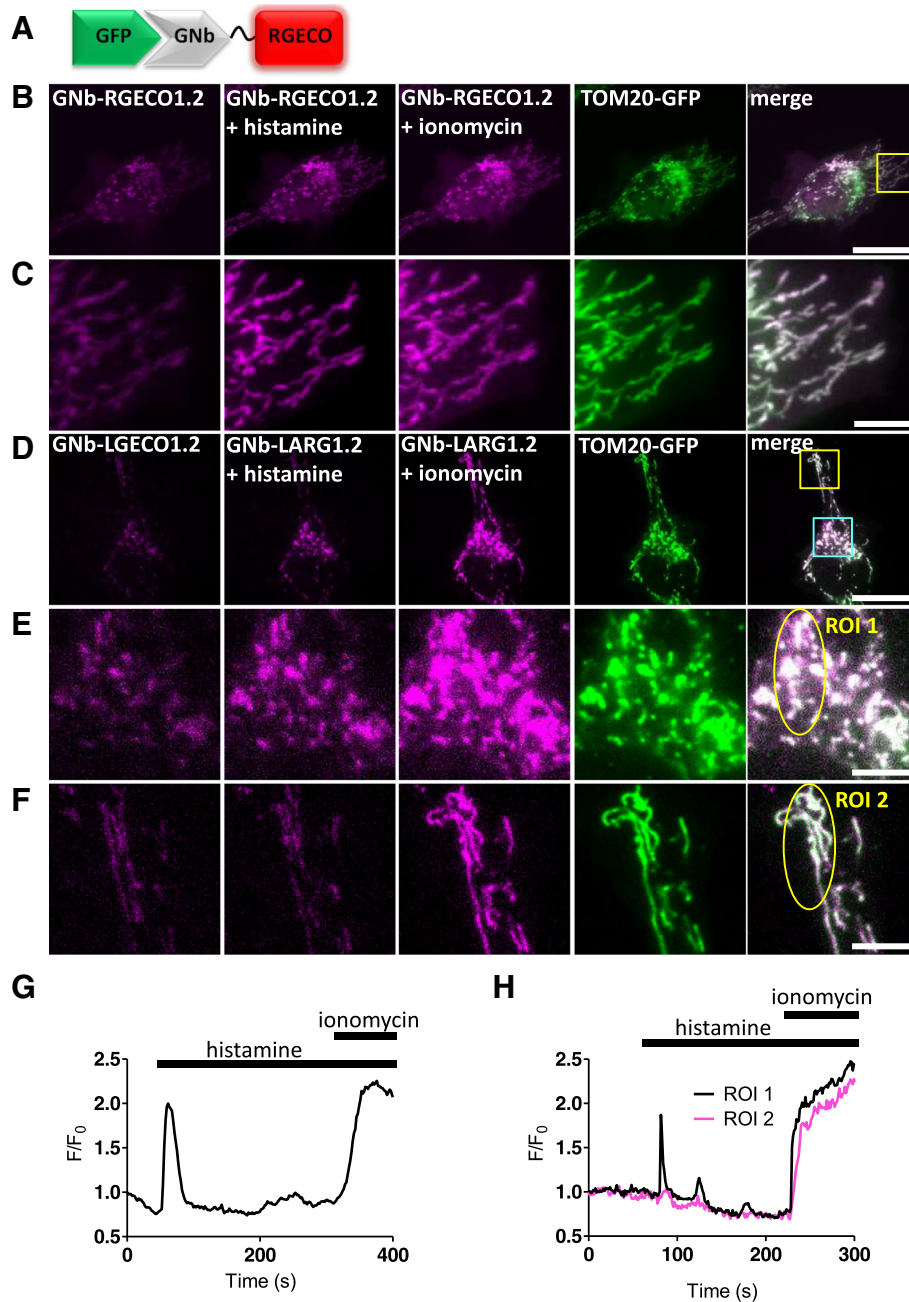


Fig. 4 Targeted GNB- Ca^{2+} sensors detect changes in $[\text{Ca}^{2+}]$ at the surface of mitochondria. **a** Schematic of GNB-RGECO fusion binding to GFP. **b, c** Representative HeLa cells co-expressing TOM20-GFP and GNb-RGECO1.2 imaged in HBS using TIRFM before and after addition of histamine (100 μM) and then ionomycin (5 μM). The TOM20-GFP images are shown after the histamine and ionomycin additions. Histamine and ionomycin evoked changes in fluorescence of GNb-RGECO1.2 at the OMM. The yellow boxed region in panel B is shown enlarged in panel c. **d-f** Similar analyses of HeLa cells co-expressing TOM20-GFP and GNb-LAR-GECO1.2 (GNb-LARG1.2). Histamine (100 μM) evoked changes in fluorescence of GNb-LARG1.2 at the OMM of mitochondria in the perinuclear region (region of interest 1 (ROI 1) in e), but not in a peripheral region (ROI 2 in f). All mitochondria responded to ionomycin (5 μM), indicating that histamine evoked local changes in $[\text{Ca}^{2+}]$ at the OMM. The cyan and yellow boxed regions in d are shown enlarged in e and f, respectively. Scale bars 10 μm (b, d) or 2.5 μm (c, e and f). **g** Timecourse of the changes in fluorescence of GNb-RGECO1.2 at the OMM evoked by histamine and ionomycin for the entire cell shown in B. **h** Fluorescence changes recorded from ROI 1 and ROI 2 in panels e and f. Results are representative of cells from 4 independent experiments

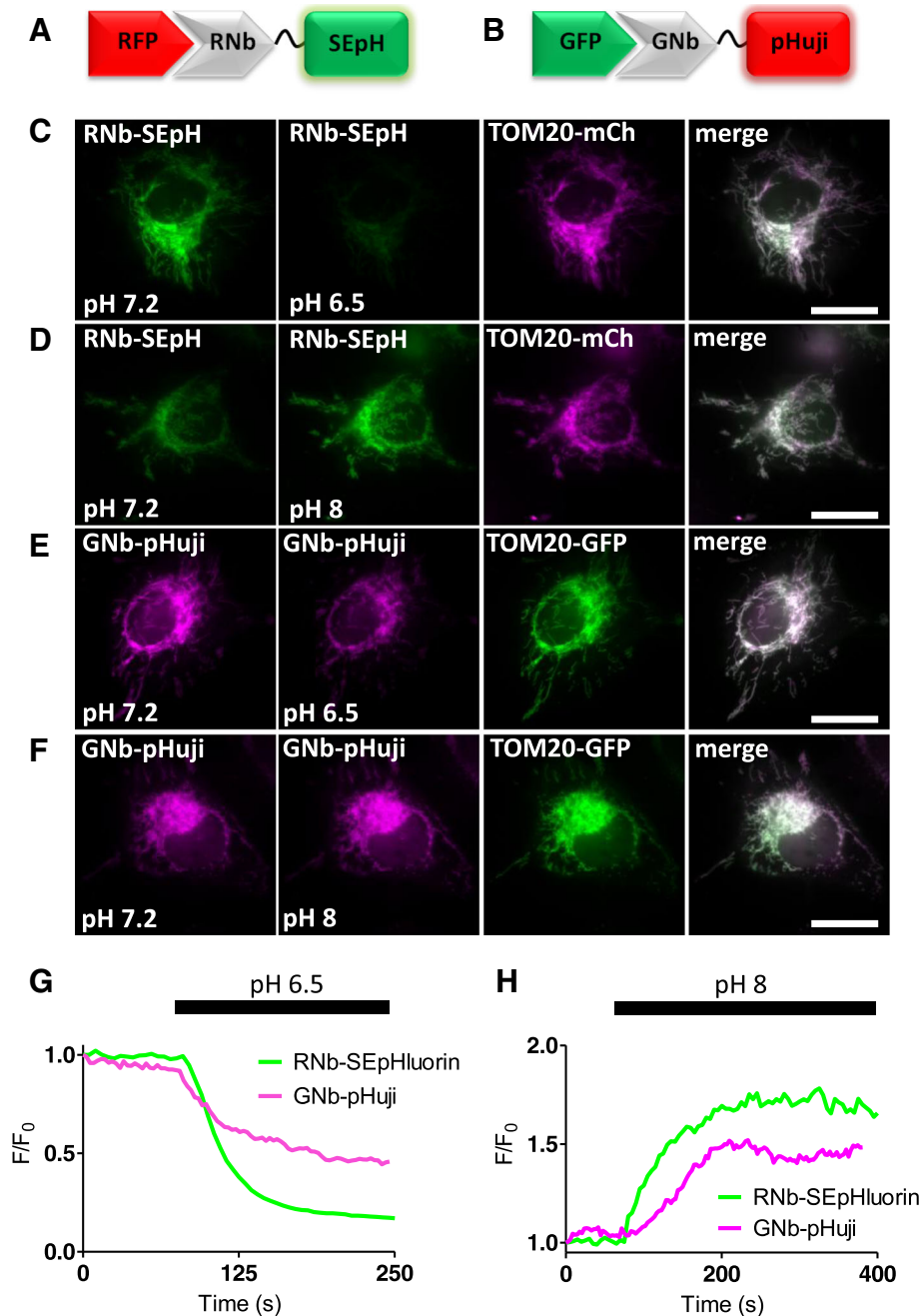


Fig. 5 Targeting H^+ sensors to RFP-tagged and GFP-tagged proteins. **a** Schematic of RNb fused to the pH sensor super-ecliptic pHluorin (RNb-SEpH) and bound to RFP. **b** Schematic of GNB-pHuji binding to RFP. **c, d** HeLa cells co-expressing RNb-SEpH and TOM20-mCh were imaged in modified HBS (MHBS) using epifluorescence microscopy and exposed to extracellular pH 6.5 (**c**) or pH 8 (**d**) in the presence of nigericin (10 μ M). Scale bars 10 μ m. **e, f** HeLa cells co-expressing GNB-pHuji and TOM20-GFP were exposed to extracellular pH 6.5 (**e**) or pH 8 (**f**) in the presence of nigericin. Scale bars 10 μ m. **g, h** Timecourse from single cells of the fluorescence changes (F/F_0) of mitochondrially targeted RNb-SEpH or GNB-pHuji evoked by the indicated manipulations of extracellular pH. Results shown are representative of 3 independent experiments

the SNAP strategy more broadly applicable to CALI applications. We demonstrate this by targeting CALI to the outer surface of lysosomes. We anticipated that CALI in this microdomain might, amongst other effects, disrupt the motility of lysosomes, which depends on their

association with molecular motors [43]. RNb-SNAPf enabled labelling of lysosomes with the CALI probe fluorescein, using the cell-permeable substrate, SNAP-Cell-fluorescein (Fig. 8a, b). Exposure to blue light then immobilized the lysosomes (Fig. 8c–f and Additional file 4: Video 3),

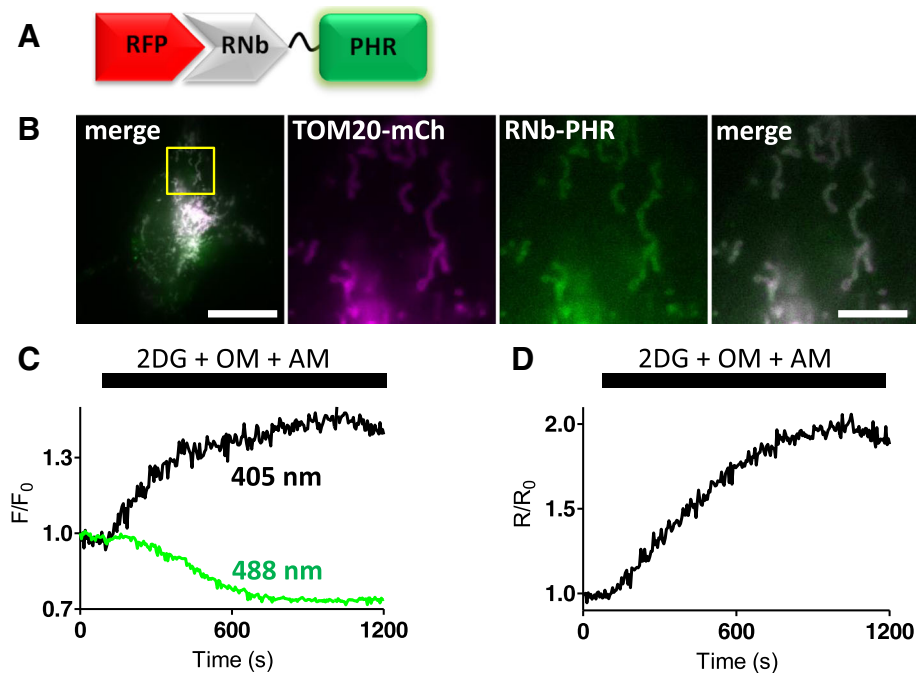


Fig. 6 Targeting an ATP/ADP sensor to RFP-tagged proteins. **a** Schematic of RNB-Perceval-HR fusion (RNB-PHR) bound to RFP. **b** HeLa cells co-expressing RNB-PHR and TOM20-mCh were imaged in HBS using epifluorescence microscopy. The yellow box indicates the region enlarged in subsequent panels. Scale bars 10 μm (main image) and 2.5 μm (enlarged images). **c, d** Changes in fluorescence for each excitation wavelength (405 and 488 nm, F/F_0) (**c**) and their ratio (R/R_0 , where $R = F_{405}/F_{488}$) (**d**) of mitochondrially targeted RNB-Perceval-HR after addition of 2-deoxyglucose (2DG, 10 mM), oligomycin (OM, 1 μM) and antimycin (AM, 1 μM). The results indicate a decrease in the ATP/ADP ratio at the OMM. Results are representative of 3 independent experiments

indicating a loss of motor-driven motility. Control experiments demonstrated that labelling cytosolic SNAPf with SNAP-Cell-fluorescein (Additional file 1: Figure S2A and S2B) had significantly less effect on lysosomal motility after exposure to blue light (Fig. 8f and Additional file 1: Figure S2C–E). These results demonstrate that nanobody-SNAPf fusions allow targeting of fluorescent dyes in live cells, which can be used for re-colouring of tagged proteins or targeted CALI.

Sequestration of proteins tagged with RFP or GFP

The fusion of GFP nanobodies to degrons allows proteasomal degradation of GFP-tagged proteins [24], but the method is slow and cumbersome to reverse. An alternative strategy is to sequester tagged proteins so they cannot fulfill their normal functions. We used two strategies to achieve this: artificial clustering and recruitment to mitochondria.

We induced artificial clustering by fusing RNB or GNB to a multimerizing protein (MP) comprising a dodecameric fragment of Ca^{2+} -calmodulin-dependent protein kinase II (CaMKII) [44], with an intervening fluorescent protein (mRFP or mCerulean) for visualization of the Nb fusion (Fig. 9a, b). RNB-mCerulean-MP caused

clustering of the ER transmembrane protein mCh-Sec61 β (Fig. 9c, d) and caused lysosomes tagged with LAMP1-mCh to aggregate into abnormally large structures (Fig. 9e, f). GNB-mRFP-MP had the same clustering effect on lysosomes labeled with LAMP1-GFP (Fig. 9g, h) and caused clustering of GFP-tagged proteins in the cytosol (calmodulin, Fig. 9i, j), nucleus and cytosol (p53, Fig. 9k, l) or ER membranes (IP₃R3, Fig. 9m, n).

For inducible sequestration, sometimes known as ‘knocksideways’ [45], we used two approaches based on heterodimerizing modules, one chemical and one optical. First, we adapted the original knocksideways method, where proteins tagged with FKBP (FK506-binding protein) are recruited by rapamycin to proteins tagged with FRB (FKBP-rapamycin-binding domain) on the OMM, and thereby sequestered. The method has hitherto relied on individual proteins of interest being tagged with FKBP [45]. RNB-FKBP and GNB-FKBP (Fig. 10a, b) extend the method to any protein tagged with RFP or GFP. For our analyses, we expressed TOM70 (an OMM protein) linked to FRB through an intermediary fluorescent protein (GFP or mCh, to allow optical identification of the fusion protein). RNB-FKBP sequestered the ER transmembrane

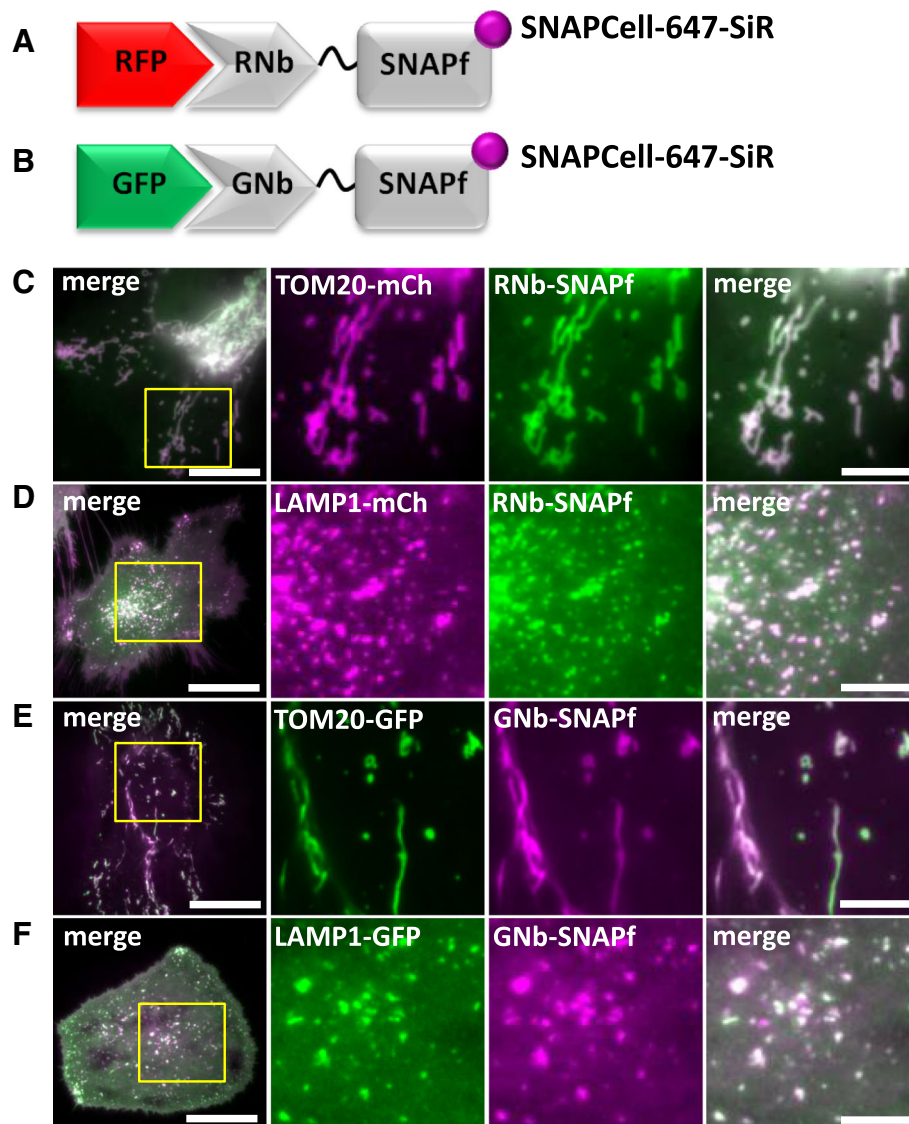


Fig. 7 Nanobody-SNAPf fusion proteins allow labelling of RFP-tagged and GFP-tagged proteins with fluorescent O^6 -benzylguanine derivatives in live cells. **a, b** Schematics of RNb-SNAPf fusion bound to RFP, and GNb-SNAPf fusion bound to GFP, after labelling with SNAP-Cell-647-SiR (magenta circles). **c-f** HeLa cells co-expressing RNb-SNAPf and mitochondrial TOM20-mCh (**c**), RNb-SNAPf and lysosomal LAMP1-mCh (**d**), GNb-SNAPf and TOM20-GFP (**e**) or GNb-SNAPf and LAMP1-GFP (**f**) were treated with SNAP-Cell-647-SiR (0.5 μ M, 30 min at 37 $^{\circ}$ C) and imaged using TIRFM. Scale bars 10 μ m (main images) or 2.5 μ m (enlarged images of yellow boxed regions). Colocalization values: RNb-SNAPf + TOM20-mCh ($r = 0.95 \pm 0.02$, $n = 6$ cells); RNb-SNAPf + LAMP1-mCh ($r = 0.84 \pm 0.06$, $n = 8$ cells); GNb-SNAPf + TOM20-GFP ($r = 0.78 \pm 0.09$, $n = 10$ cells); and GNb-SNAPf + LAMP1-GFP ($r = 0.85 \pm 0.10$, $n = 11$ cells)

protein mCh-Sec61 β at the OMM (TOM70-GFP-FRB) within seconds of adding rapamycin (Additional file 5: Video 4) and rapidly depleted mCh-Sec61 β from the rest of the ER (Fig. 10c–e). After addition of rapamycin, GNb-FKBP rapidly sequestered endogenous IP $_3$ R1 tagged with GFP (GFP-IP $_3$ R1) [7] (Fig. 10f, g, and Additional file 6: Video 5) and cytosolic GFP-tagged calmodulin (Fig. 10h and Additional file 7: Video 6) at mitochondria expressing TOM70-mCh-FRB. Rapamycin caused no sequestration in the absence of the nanobody fusions (Additional file 1: Figure S3).

To make sequestration reversible and optically activated, we adapted the light-oxygen-voltage-sensing domain (LOV2)/Zdark (zdk1) system in which light induces dissociation of LOV2-zdk1 hetero-dimers [46]. Because this system is operated by blue light at intensities lower than required for imaging GFP [46], it is most suitable for use with red fluorescent tags. RNb-zdk1 (Fig. 11a) sequestered cytosolic mCh on the OMM in cells expressing TOM20-LOV2, and blue laser light rapidly and reversibly redistributed mCh to the cytosol (Fig. 11b, c).

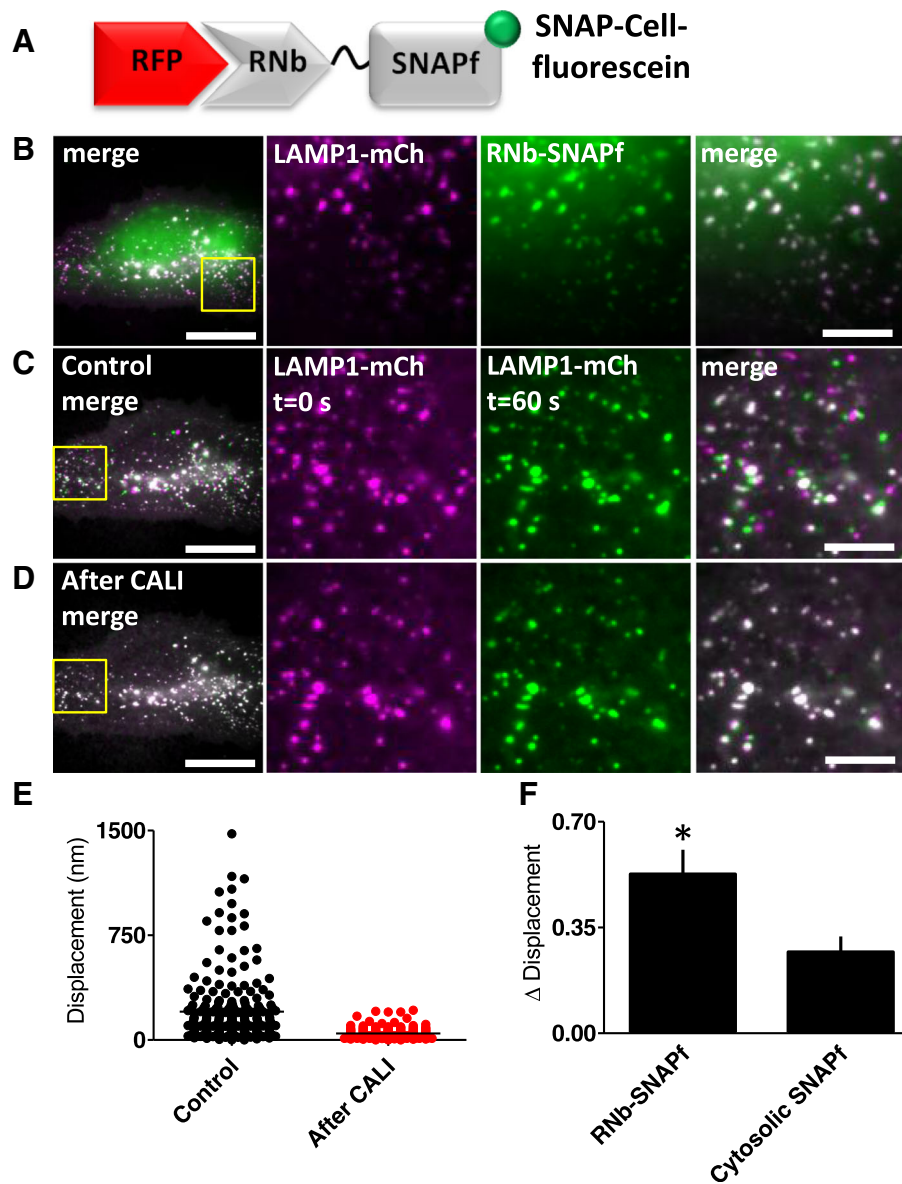


Fig. 8 Targeting CALI to lysosomes using RNb-SNAPf reduces lysosomal motility. **a** Schematic of RNb-SNAPf after labelling with SNAP-Cell-fluorescein (green circle) and bound to RFP. **b** HeLa cells co-expressing LAMP1-mCh and RNb-SNAPf were incubated with SNAP-Cell-fluorescein (0.5 μM, 30 min, 37 °C), which labelled lysosomes (colocalization values, $r = 0.73 \pm 0.02$, $n = 6$ cells), and imaged using TIRFM. **c, d** Cells were then exposed to 488-nm light for 3 s to induce CALI. TIRFM images show a representative cell at different times before (**c**) and after (**d**) CALI, with the image at $t = 0$ s shown in magenta and the image at $t = 60$ s in green. White in the merged images from the two different times indicates immobile lysosomes, while green and magenta indicate lysosomes that moved in the interval between images. Yellow boxes show regions enlarged in subsequent images. Scale bars 10 μm (main images) and 2.5 μm (enlargements). For clarity, images were auto-adjusted for brightness and contrast (ImageJ) to compensate for bleaching of mCh during tracking and CALI. **e** Effect of CALI on the displacements of individual lysosomes, determining by particle-tracking (TrackMate), during a 60-s recording from a representative cell (images taken every 1 s; mean values shown by bars). **f** Summary data (mean \pm SEM, $n = 6$ cells from 6 independent experiments) show the mean fractional decrease in displacement (Δ displacement) due to CALI in cells expressing RNb-SNAPf or cytosolic SNAPf (see Additional file 1: Figure S2). The fractional decrease in displacement for each cell was defined as $(MD_{pre} - MD_{post}) / MD_{pre}$, where MD_{pre} and MD_{post} are the mean displacement of all tracked particles in 60 s before and after CALI. * $P < 0.05$, unpaired Student's t test

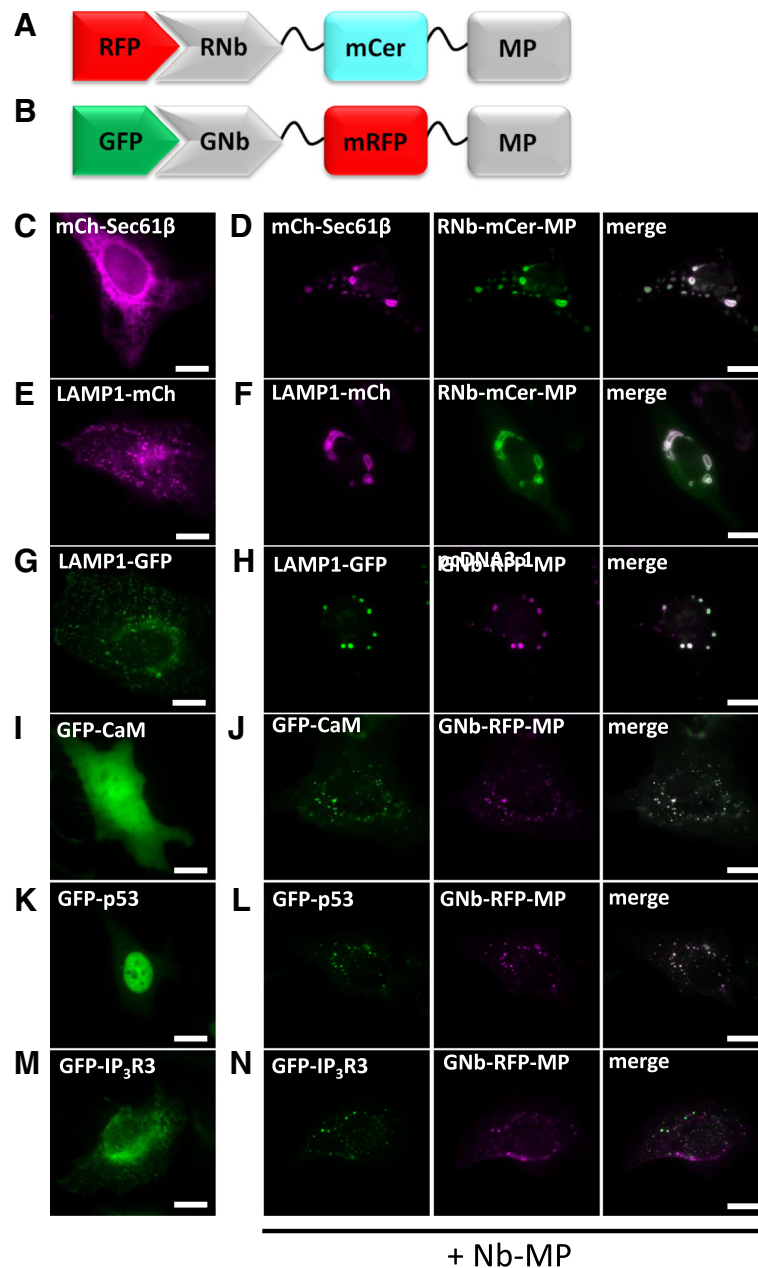


Fig. 9 Clustering of RFP-tagged and GFP-tagged proteins and organelles using RNb-mCerulean-MP and GNb-mRFP-MP. **a** Schematic of RNb-mCerulean-MP fusion bound to RFP. **b** Schematic of GNb-mRFP-MP fusion bound to GFP. **c–f** HeLa cells expressing RFP-tagged proteins in the absence (**c, e**) or presence (**d, f**) of co-expressed RNb-mCerulean-MP (RNb-mCer-MP) were imaged using epifluorescence microscopy. **g–n** HeLa cells expressing GFP-tagged proteins in the absence (**g, i, k, m**) or presence (**h, j, l, n**) of co-expressed GNb-mRFP-MP were imaged using epifluorescence microscopy. Results are representative of at least 5 cells, from at least 3 independent experiments. Scale bars 10 μ m

Inducible recruitment of tagged proteins to membrane contact sites

The ability of Nb-FKBP fusions to recruit membrane proteins to FRB-tagged targets suggested an additional application: revealing contact sites between membrane-bound organelles. ER-mitochondrial membrane contact sites (MCS) have been much studied [47], but contacts between the PM and mitochondria, which are less extensive [48],

have received less attention. In HeLa cells co-expressing the PM β_2 -adrenoceptor tagged with mCh (β_2 AR-mCh), TOM20-GFP-FRB and RNb-FKBP, rapamycin caused rapid recruitment of β_2 AR-mCh within the PM to mitochondria at discrete puncta that grew larger with time (Fig. 12a–e and Additional file 8: Video 7). Recruitment was not seen in the absence of co-expressed RNb-FKBP (Fig. 12f). Rapamycin also triggered similar punctate

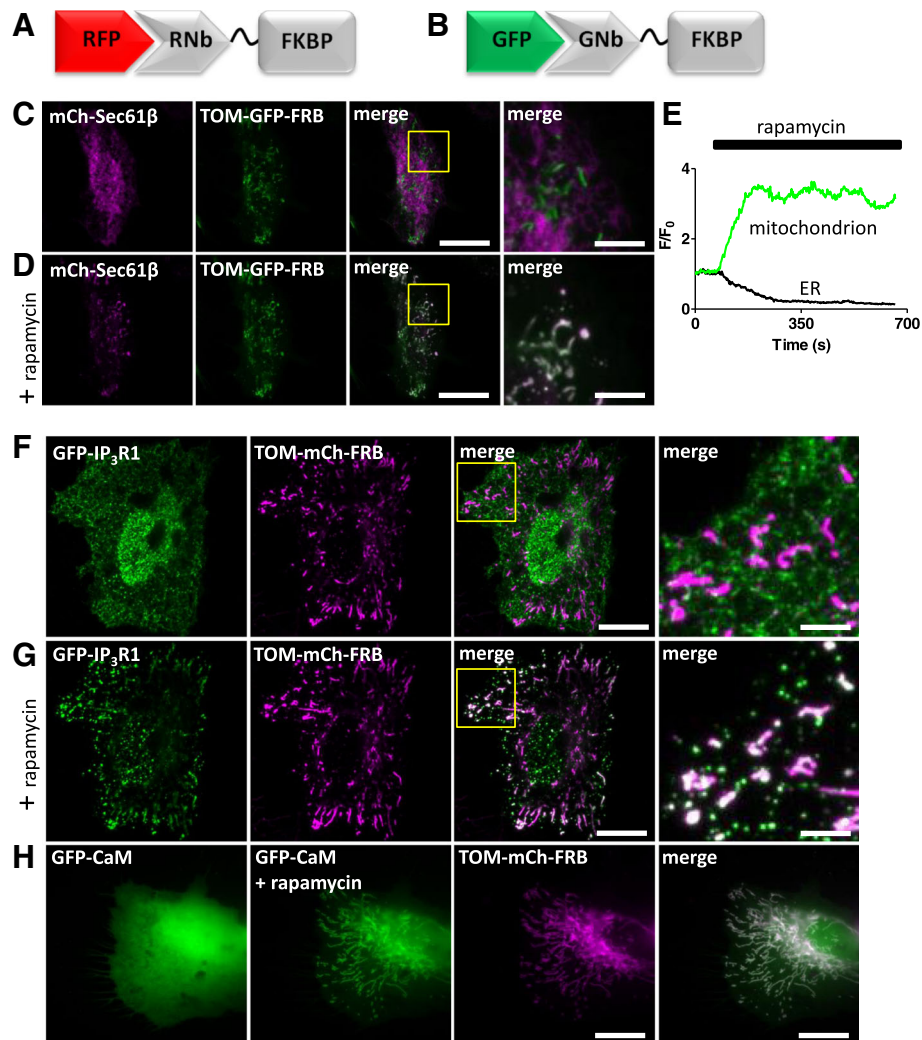
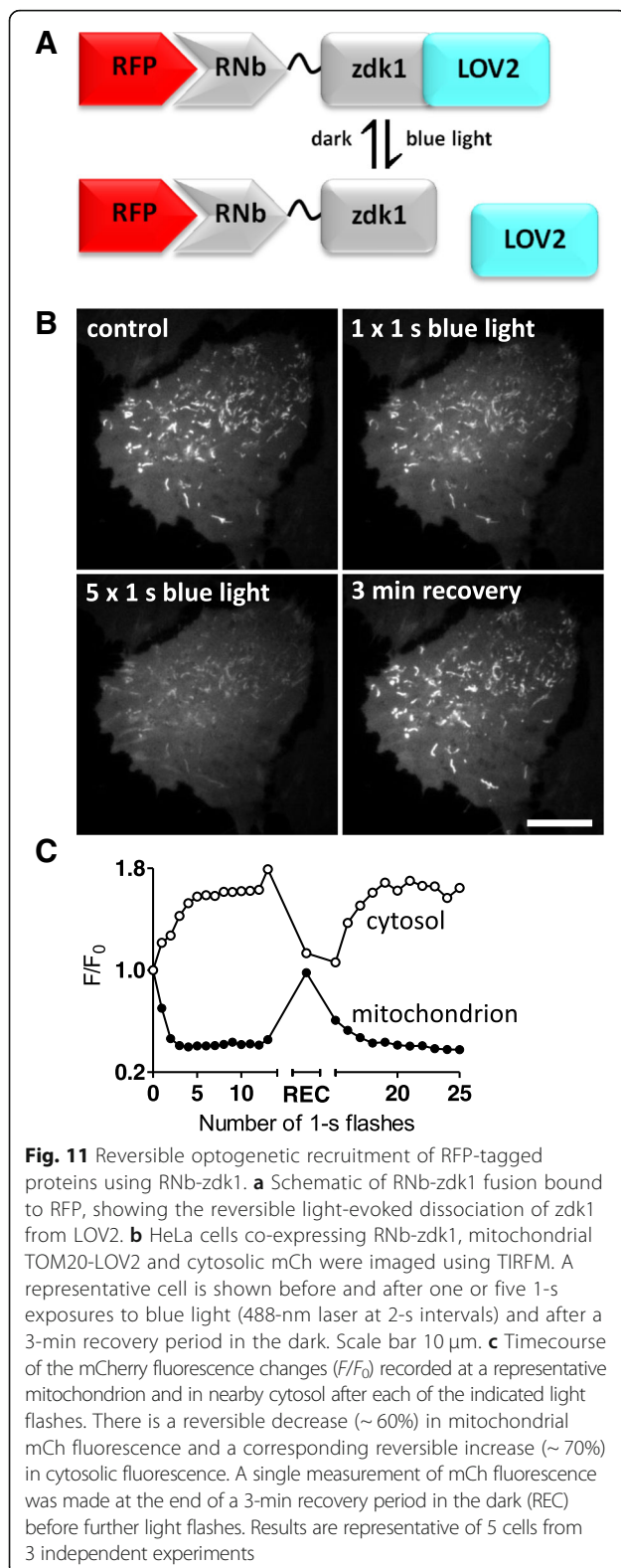


Fig. 10 RNb-FKBP inducibly recruits ER transmembrane proteins to mitochondria. **a** Schematic of RNb-FKBP bound to RFP. **b** Schematic of GNB-FKBP bound to GFP. **c, d** HeLa cells co-expressing RNb-FKBP, mitochondrial TOM70-GFP-FRB and mCh-Sec61 β were imaged using TIRFM. A representative cell ($n = 7$) is shown before (**c**) and after (**d**) treatment with rapamycin (100 nM, 10 min). The boxed region is enlarged in subsequent images. Scale bars 10 μ m (main images) and 2.5 μ m (enlargements). **e** Timecourse of mCh-Sec61 β fluorescence changes (F/F_0) evoked by rapamycin recorded at a representative mitochondrion and in nearby reticular ER. Results show $\sim 80\%$ loss of fluorescence from the ER devoid of mitochondrial contacts. **f, g** HeLa cells co-expressing endogenously tagged GFP-IP $_3$ R1, GNB-FKBP and mitochondrial TOM70-mCh-FRB were imaged using TIRFM. A representative cell ($n = 6$) is shown before (**f**) and after (**g**) treatment with rapamycin (100 nM, 10 min). The boxed region is enlarged in subsequent images. Scale bars 10 μ m (main images) and 2.5 μ m (enlargements). **h** HeLa cells co-expressing GFP-calmodulin (GFP-CaM), GNB-FKBP and TOM20-mCh-FRB were imaged using epifluorescence microscopy. A representative cell ($n = 3$) is shown before and after treatment with rapamycin (100 nM, 10 min). The image for TOM-mCh-FRB is shown in the presence of rapamycin. Scale bar 10 μ m

accumulation of β_2 AR at mitochondria in COS-7 cells expressing β_2 AR-GFP, TOM20-mCh-FRB and GNB-FKBP (Additional file 1: Figure S4). In similar analyses of ER-mitochondria and PM-mitochondria MCS, the initial punctate co-localization of proteins was shown to report native MCS, which grew larger with time as rapamycin zipped the proteins together [48]. Our results are consistent with that interpretation. In most cases, β_2 AR were recruited to only one or two discrete sites on each mitochondrion, which expanded during prolonged incubation with rapamycin, but without the appearance of new sites

(Fig. 12d, e, and Additional file 1: Figure S4). Rapamycin had no evident effect on recruiting new mitochondria to the PM, but it did cause accumulation of tagged TOM70 at MCS and depletion of TOM70 from the rest of each mitochondrion, indicating mobility of TOM70 within the OMM (Additional file 1: Figure S4). Our results suggest that inducible crosslinking using RNb-FKBP or GNB-FKBP identifies native MCS between mitochondria and PM, with each mitochondrion forming only one or two MCS with the PM. We have not explored the functional consequences of these restricted MCS, but we speculate



that they may identify sites where proteins involved in communication between the PM and mitochondria are concentrated, facilitating, for example, phospholipid transfer [49], the generation of ATP microdomains [50], or Ca^{2+} exchanges between mitochondria and store-operated Ca^{2+} entry (SOCE) [51] or PM Ca^{2+} -ATPases [52].

We next tested whether PM proteins could be recruited to the MCS between ER-PM that are important for SOCE and lipid transfer [53]. In response to rapamycin, mCh-Orai1, the PM Ca^{2+} channel that mediates SOCE [54], was recruited by RNb-FKBP to ER-PM MCS labelled with the marker GFP-MAPPER-FRB [55] (Fig. 13a, b). Recruitment was not observed in the absence of RNb-FKBP (Fig. 13c). We conclude that the method identifies native ER-PM MCS during the initial phase of Nb recruitment, and the Nb subsequently exaggerates these MCS.

One of the least explored MCS is that between lysosomes and mitochondria [56]. Recent evidence shows that these MCS control the morphology of both organelles [57] and probably mediate the exchange of cholesterol and other metabolites between them [58]. We assessed whether the nanobody fusions could be used to inducibly recruit lysosomes to mitochondria. GNB-FKBP enabled recruitment of lysosomes labelled with LAMP1-GFP to mitochondria labelled with TOM20-mCh-FRB, in response to rapamycin (Fig. 14a–c). Lysosomes were not recruited to mitochondria in the absence of GNB-FKBP (Fig. 14d).

Crosslinking RFP-tagged and GFP-tagged proteins

We generated a dimeric nanobody (GNb-RNb) that binds simultaneously to GFP and RFP (Fig. 15a) and demonstrated its utility by crosslinking a variety of GFP-tagged and RFP-tagged proteins. Cytosolic GFP, normally diffusely distributed in the cytosol (data not shown), was recruited to nuclei by H2B-mCh (Fig. 15b) or to mitochondria by TOM20-mCh (Fig. 15c). In the presence of GNB-RNb, mCh-Orai1 and endogenously tagged GFP-IP₃R1 formed large co-clusters (Fig. 15d) that differed markedly from the distributions of GFP-IP₃R1 (Fig. 10f) and mCh-Orai1 (Fig. 13) in the absence of crosslinking. Consistent with earlier results (Fig. 12 and Additional file 1: Figure S4), β_2 AR-mCh, which is normally diffusely distributed in the PM, formed mitochondria-associated puncta when cross-linked to mitochondria expressing TOM20-GFP (Fig. 15e). Whole organelles could also be crosslinked. Co-expression of LAMP1-GFP and LAMP1-mCh labelled small, mobile lysosomes in control cells (Fig. 15f), while additional co-expression of GNB-RNb caused accumulation of lysosomes into large clusters (Fig. 15g).

This crosslinking of GFP and RFP was made rapidly inducible with an RNb-FRB fusion that hetero-dimerizes with GNB-FKBP in the presence of rapamycin (Fig. 16a). Co-expression of GNB-FKBP with RNb-FRB in cells

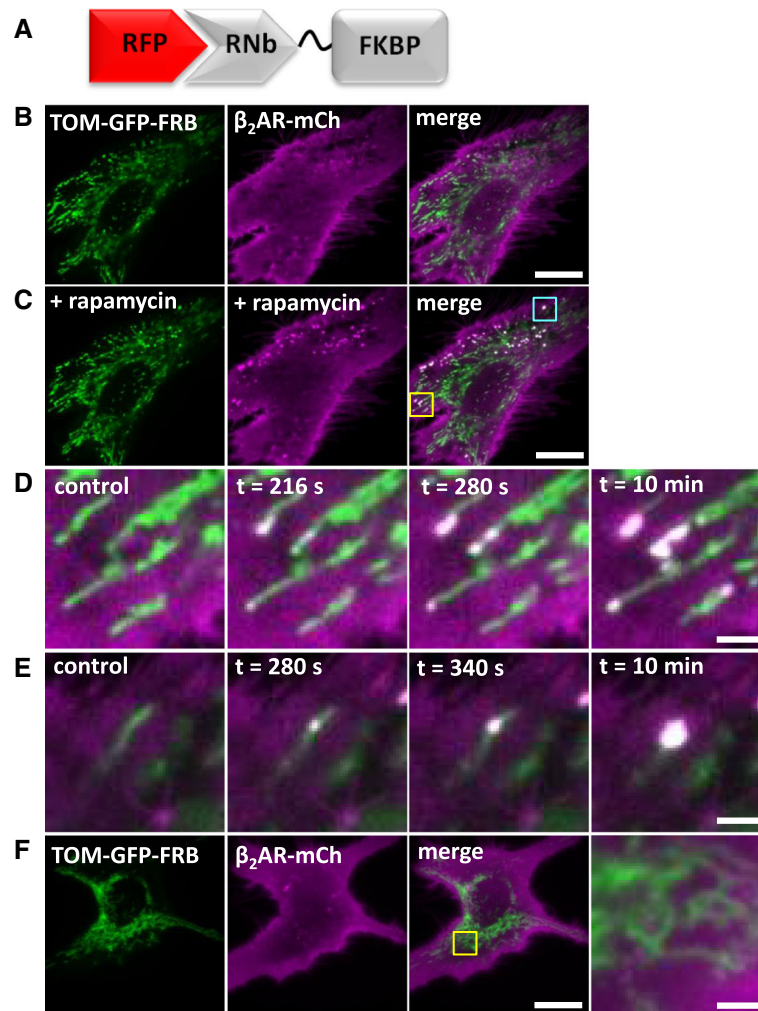


Fig. 12 Recruitment of proteins to native PM-mitochondria MCS using RNb-FKBP. **a** Schematic of RNb-FKBP fusion bound to RFP. **b, c** HeLa cells co-expressing RNb-FKBP, mitochondrial TOM70-GFP-FRB and β_2 AR-mCh were imaged using TIRFM before (**b**) and after (**c**) treatment with rapamycin (100 nM, 10 min). Scale bar 10 μ m. **d, e** Enlarged images from C of the yellow box (**d**) and cyan box (**e**) show punctate recruitment of β_2 AR-mCh to individual mitochondria at the indicated times after addition of rapamycin. Scale bars 1.25 μ m. **f** TIRFM images of HeLa cells co-expressing mitochondrial TOM70-GFP-FRB and β_2 AR-mCh in the presence of rapamycin (100 nM, 10 min) show no recruitment in the absence of co-expressed RNb-FKBP. The yellow box shows a region enlarged in the subsequent image. Scale bars 10 μ m (main images) and 2.5 μ m (enlargement). Results (**b-f**) are representative of 5 independent experiments

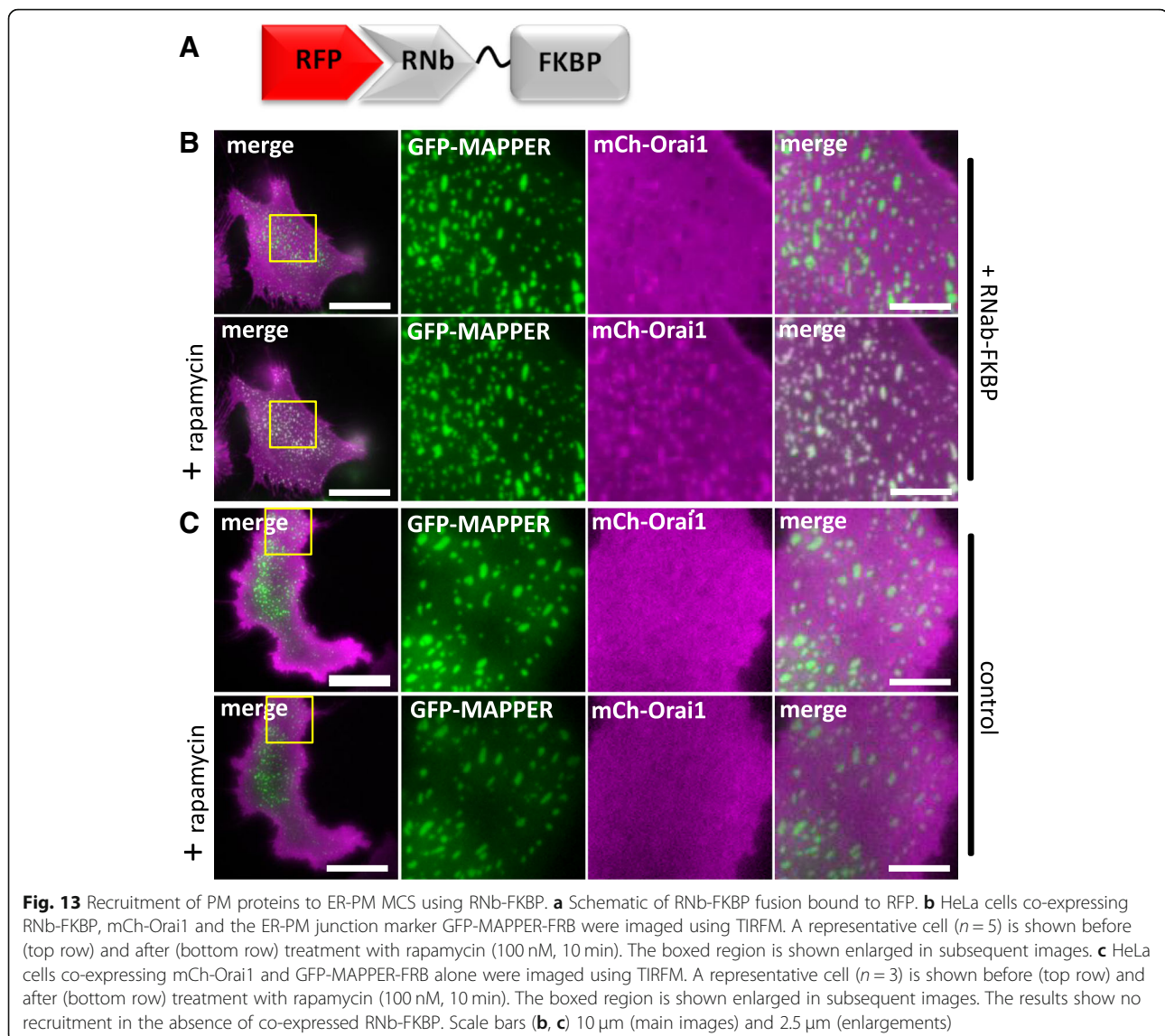
co-expressing TOM20-GFP and mCh-Sec61 β led to rapid colocalization of GFP and mCh after addition of rapamycin (Fig. 16b, c, and Additional file 9: Video 8). Similar results were obtained with RNb-FKBP and GNb-FRB (Additional file 1: Figure S5). We conclude that GNb-FKBP and RNb-FRB provide a rapidly inducible system for crosslinking any GFP-tagged protein to any RFP-tagged protein.

Targeting secretory compartments with luminal nanobodies

GNb and RNb were directed to the lumen of the secretory pathway by addition of an N-terminal signal sequence, giving ssGNb and ssRNb. Targeting of ssGNb-mCh to the

Golgi, ER network or ER-PM MCS was achieved by co-expression of organelle markers with luminal FP tags (Fig. 17a, b). In each case, there was significant colocalization of green and red proteins. Similar targeting of ssRNb-GFP to the ER network or ER-PM MCS was achieved by co-expression with mCh-tagged luminal markers of these organelles (Fig. 17c, d). These results demonstrate that ssGNb and ssRNb fusions can be directed to the lumen of specific compartments of the secretory pathway.

Fluorescent Ca^{2+} sensors targeted to the lumen of the entire ER [59, 60] are widely used and have considerably advanced our understanding of Ca^{2+} signalling [61, 62]. Fluorescent Ca^{2+} sensors targeted to ER sub-compartments



and the secretory pathway have received less attention but have, for example, been described for the Golgi [63, 64]. Our nanobody methods suggest a generic approach for selective targeting of luminal Ca^{2+} indicators. Fusion of ssRNb to GCEPIA1 or GEMCEPIA [60] provided ssRNb-GCEPIA1 and ssRNb-GEMCEPIA (Fig. 18a). These fusions were targeted to the luminal aspect of ER-PM junctions by co-expression with mCh-MAPPER [7] (Fig. 18c, d). Fusion of ssGNb to the low-affinity Ca^{2+} sensors LAR-GECO1 [59] or RCEPIA1 [60] provided ssGNb-LARGECO1 and ssGNb-RCEPIA1 (Fig. 18b). These fusions allowed targeting to ER-PM junctions labelled with GFP-MAPPER (Fig. 18e, f). The targeted Ca^{2+} sensors responded appropriately to emptying of intracellular Ca^{2+} stores by addition of ionomycin in Ca^{2+} -free medium (Fig. 18g–k). These results confirm that Ca^{2+} sensors targeted to a physiologically important ER

sub-compartment, the ER-PM junctions where SOCE occurs, report changes in luminal $[\text{Ca}^{2+}]$. Our results demonstrate that nanobody fusions can be targeted to luminal sub-compartments of the secretory pathway and they can report $[\text{Ca}^{2+}]$ within physiologically important components of the ER.

Discussion

The spatial organization of the cell interior influences all cellular activities, and it is a recurrent theme in intracellular signalling [65, 66]. Hence, tools that can visualize and manipulate the spatial organization of intracellular components are likely to find widespread application. We introduce a toolkit of plasmids encoding functionalized nanobodies against common FP tags, including CFP, GFP, YFP and RFPs (Fig. 1). Use of this toolkit is supported by genome-wide collections of plasmids, cells and organisms

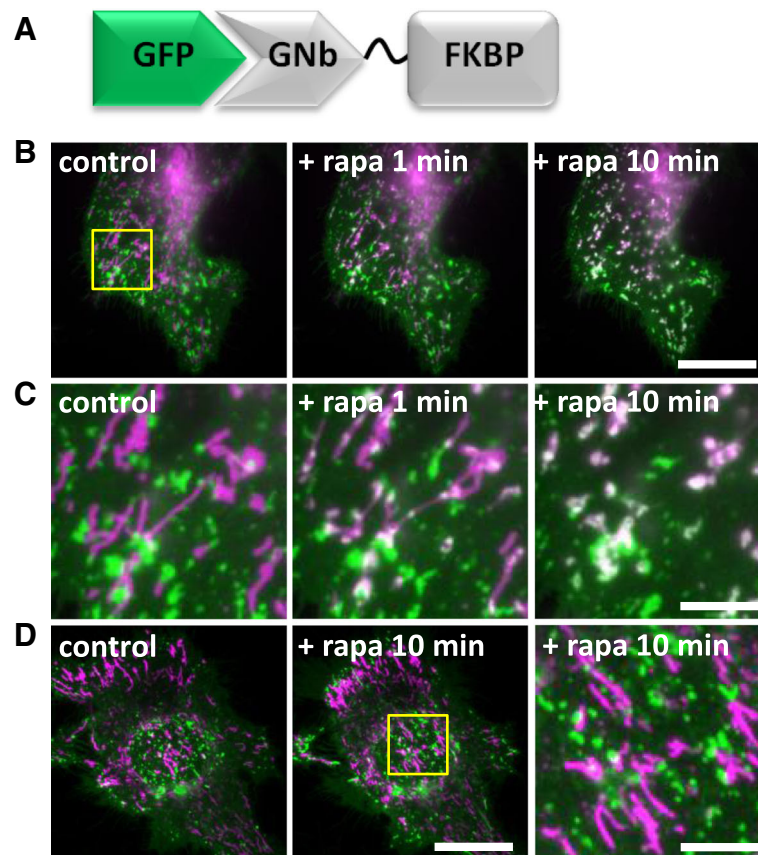


Fig. 14 Inducible recruitment of lysosomes to mitochondria using GNB-FKBP. **a** Schematic of GNB-FKBP fusion bound to GFP. **b** HeLa cells co-expressing mitochondrial TOM70-mCh-FRB (magenta), lysosomal LAMP1-GFP (green) and GNB-FKBP were imaged using TIRFM. Merged images of a representative cell ($n = 5$) are shown before and at times after treatment with rapamycin (rapa, 100 nM). Scale bar 10 μm . **c** Enlargements of the boxed region in **b**. Scale bar 2.5 μm . **d** HeLa cells co-expressing TOM70-mCh-FRB (magenta) and lysosomal LAMP1-GFP (green) were imaged using TIRFM. A representative cell ($n = 3$) is shown before and after treatment with rapamycin (100 μM , 10 min); there is no recruitment in the absence of co-expressed GNB-FKBP. The yellow box shows a region enlarged in the subsequent image. Scale bars 10 μm (main images) and 2.5 μm (enlargement)

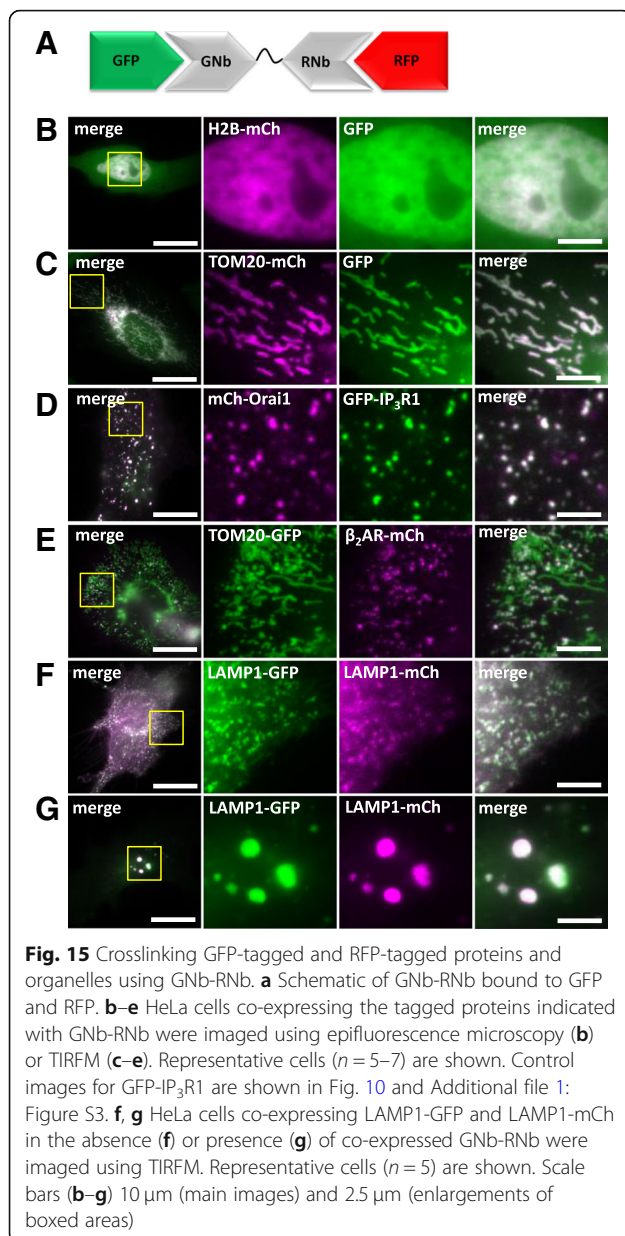
expressing proteins tagged with GFP and RFP [10–17, 19] and by facile methods for heterologous expression of tagged proteins or editing of endogenous genes to encode FP tags [5, 6]. The functionalized nanobodies provide new approaches to studying intracellular signalling in live cells.

Our toolkit expands the repertoire of functionalized RFP-binding nanobodies, which are less developed than their GFP-binding counterparts [67]. The RNb fusions provide new opportunities to use RFP, which often has advantages over GFP. For example, RFP is spectrally independent from blue-green sensors, which are usually superior to their red counterparts [30, 32]; from the CALI probe, fluorescein; and from optogenetic modules, which are often operated by blue-green light [68].

Nanobody-sensor fusions allow targeting of sensors to specific proteins and organelles (Figs. 2, 3, 4, 5 and 6) and will aid visualization of signalling within cellular microdomains. Fusion of nanobodies to the Ca^{2+} sensors G-GECO1.2, R-GECO1.2 and LAR-GECO1.2 [30] (Figs. 3

and 4), which have relatively low affinities for Ca^{2+} (K_D values of 1.2 μM , 1.2 μM and 10 μM , respectively), should facilitate selective detection of the relatively large, local rises in $[\text{Ca}^{2+}]_c$ that are important for cell signalling [27]. The GEM-GECO Ca^{2+} sensor [30], H^+ sensors [31, 32] and ATP/ADP sensors [33] used for nanobody fusions are poised to detect fluctuations of their ligands around resting concentrations in the cell (Figs. 4, 5 and 6).

Relative to direct fusions of sensors to proteins of interest, nanobody-sensor fusions have several advantages. Firstly, the generic nanobody toolkit (Fig. 1) can be combined with collections of FP-tagged proteins to provide many combinations; each would otherwise require the expression of a unique construct that may or may not function normally. Secondly, each sensor is attached to the same entity (nanobody), which binds to the same partner (FP). Since the biophysical and biochemical properties of sensors may be influenced by their fusion partners, this



provides greater confidence that sensors despatched to different locations will respond similarly to their analyte.

Nanobodies allow re-colouring of FPs with alternative fluorophores that may have advantageous properties. For example, re-colouring of RFP-tagged proteins with RNB-GFP (Fig. 2b) enables visualization of organelles with GFP, which has enhanced photophysical properties relative to RFPs. Nanobody-SNAPf fusions can be used to attach fluorescent dyes, including CALI probes and far-red fluorophores, to FP tags (Figs. 7 and 8). Longer excitation wavelengths cause less phototoxicity and allow greater penetration through tissue, which may be useful in studies of transgenic organisms and tissues. We also envisage live-cell applications in pulse-chase

analyses and using super-resolution microscopy, Förster resonance energy transfer (FRET) and fluorescence lifetime imaging.

Membrane-permeant forms of the SNAP ligand, O⁶-benzylguanine, are available conjugated to conventional Ca²⁺ indicators (Fura-2FF, Indo-1 and BOCA-1), which are brighter than genetically encoded indicators [69–71]; to derivatives of the two-photon fluorophore naphthalimide [72]; to the hydrogen peroxide sensor nitrobenzoylcarbonylfluorescein [73]; and to reversible chemical dimerizers [74, 75]. Nanobody-SNAPf fusions will allow facile targeting of these modules to any protein or organelle tagged with RFP or GFP.

Crosslinking methods have many applications in cell biology, including stabilizing protein interactions (e.g. for pull-downs), identifying and manipulating MCS, enforcing protein interactions (e.g. receptor dimerization), redirecting proteins to different subcellular locations (e.g. knocksideways) and many more. Functionalized nanobodies provide many additional opportunities to regulate protein associations. The nanobody-FKBP/FRB fusions, for example, allow rapid rapamycin-mediated crosslinking of any pair of proteins tagged with GFP/RFP or tagged with either FP and any of the many proteins already tagged with FKBP or FRB [76] (Figs. 10, 12, 13, 14, 15, and 16). Nanobody-FKBP fusions may allow crosslinking to SNAP-tagged proteins [75], and the nanobody-SNAPf fusions to HaloTag-tagged proteins [74] and FKBP-tagged proteins [75]. RNB-zdk1 fusions allow photo-inducible crosslinking of RFP-tagged proteins to LOV-tagged proteins [46] (Fig. 11). Nanobodies that crosslink GFP-tagged proteins to RFP-tagged proteins (GNb-RNB; and the GNB-FKBP/RNB-FRB and GNB-FRB/RNB-FKBP pairings) may have the most applications, as they can take the fullest advantage of the numerous combinations of existing RFP and GFP-tagged proteins (Figs. 15 and 16).

Functionalized nanobodies directed to luminal compartments of the secretory pathway would provide useful tools, but they are under-developed. Their potential is shown by nanobodies retained within the ER, which restrict onward trafficking of target proteins and inhibit their function [77]. We show that functionalized nanobodies, including nanobody-Ca²⁺ sensors, can be directed to sub-compartments of the secretory pathway (Figs. 17 and 18). Luminal Ca²⁺ provides a reservoir within the ER, Golgi and lysosomes that can be released by physiological stimuli to generate cytosolic Ca²⁺ signals [78, 79]. Compartmentalization of Ca²⁺ stores within the ER [63] and Golgi [79] adds to the complexity of luminal Ca²⁺ distribution in cells. Furthermore, luminal Ca²⁺ itself regulates diverse aspects of cell biology, including SOCE [54], sorting of cargo in the Golgi [80], binding of ERGIC-53 to cargoes within the ER-Golgi intermediate compartment (ERGIC) [81], and exocytosis of neurotransmitters by

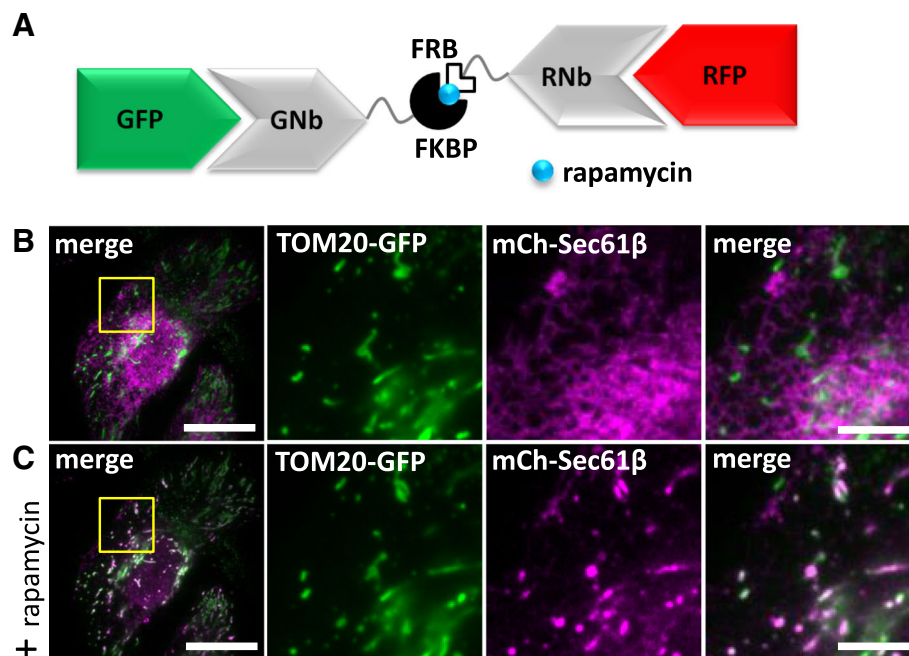


Fig. 16 Inducible crosslinking of RFP-tagged and GFP-tagged proteins with GNb-FKBP and RNb-FRB. **a** Schematic of the nanobody fusions used, with rapamycin shown as a blue sphere. **b, c** HeLa cells co-expressing GNb-FKBP, RNb-FRB, TOM20-GFP and mCh-Sec61β were imaged using TIRFM. A representative cell ($n = 3$) is shown before (**b**) and after (**c**) treatment with rapamycin (100 nM, 10 min). Scale bars 10 μm (main images) and 2.5 μm (enlargements of boxed areas)

secretory vesicles [82, 83]. Hence, there is a need for tools that can effectively report luminal $[\text{Ca}^{2+}]$ within this complex luminal environment. The luminal nanobody- Ca^{2+} sensors detected changes in luminal $[\text{Ca}^{2+}]$ at the ER-PM MCS where SOCE occurs (Fig. 18).

In addition to nanobodies, other protein-based binders, including single-domain antibodies, designed ankyrin-repeat proteins (DARPin), affimers, anticalins, affibodies and monobodies have been developed to recognise many important intracellular proteins [2, 84–86]. These binding proteins can be easily transplanted into the fusion scaffolds described to maximize their exploitation.

Conclusions

We present a toolkit of plasmids encoding functionalized nanobodies directed against common fluorescent protein tags, which will allow a wide range of applications and new approaches to studying intracellular signalling in live cells. We illustrate some applications and demonstrate, for example, that IP_3 receptors deliver Ca^{2+} to the OMM of only some mitochondria and that MCS between mitochondria and the plasma membrane occur at only one or two sites on each mitochondrion.

Materials and methods

Materials

Human fibronectin was from Merck Millipore. Ionomycin was from Apollo Scientific (Stockport, UK). Rapamycin

was from Cambridge Bioscience (Cambridge, UK). SNAP substrates were from New England Biolabs (Hitchin, UK). Other reagents, including histamine and nigericin, were from Sigma-Aldrich.

Plasmids

Sources of plasmids encoding the following proteins were mCherry-C1 (Clontech #632524); mCherry-N1 (Clontech #632523); EGFP-N1 (Clontech #6085-1); GFP-ERcyt, mCherry-ERcyt and mTurquoise2-ERcyt (GFP, mCherry or mTurquoise2 targeted to the cytosolic side of the ER membrane via the ER-targeting sequence of the yeast UBC6 protein) [87]; mCherry-ERlumen (Addgene #55041, provided by Michael Davidson); LAMP1-mCherry [88]; TPC2-mRFP [89]; TOM20-mCherry (Addgene #55146, provided by Michael Davidson); CIB1-mRFP-MP (Addgene #58367) [44]; CIB1-mCerulean-MP (Addgene #58366) [44]; H2B-GFP (Addgene #11680) [90]; TOM20-LOV2 (Addgene #81009) [46]; mCherry-Sec61β [91]; GFP-MAPPER [55]; GFP-CaM (Addgene #47602, provided by Emanuel Strehler); TOM70-mCherry-FRB (pMito-mCherry-FRB, Addgene #59352) [92]; pmTurquoise2-Golgi (Addgene #36205) [93]; pTriEx-mCherry-zdk1 (Addgene #81057) [46]; pTriEx-NTOM20-LOV2 (Addgene #81009) [46]; $\beta_2\text{AR}$ -mCFP (Addgene #38260) [94]; pCMV-G-CEPIA1er (Addgene #58215) [60]; pCMV-R-CEPIA1er (Addgene #58216) [60]; pCIS-GEMCEPIA1er (Addgene #58217) [60]; CMV-ER-LAR-

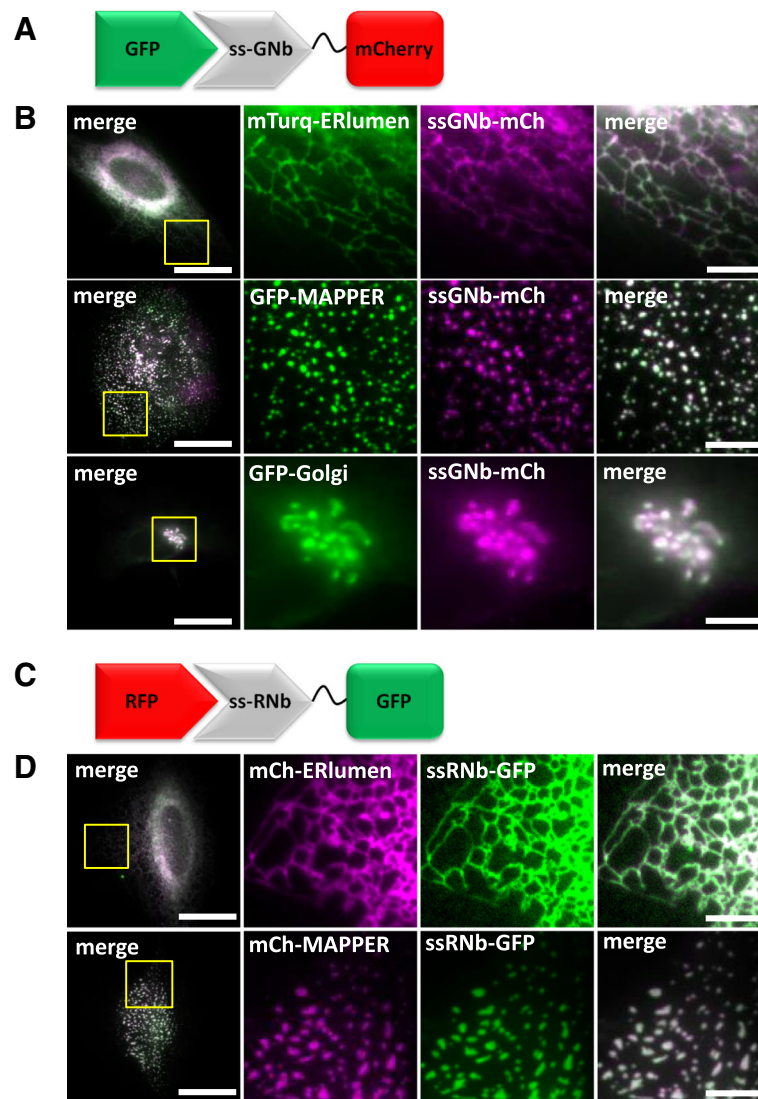


Fig. 17 Nanobody fusions can be targeted to different luminal compartments of the secretory pathway. **a** Schematic of ssGNb-mCh bound to GFP. **b** HeLa cells co-expressing ssGNb-mCh and either the luminal ER marker mTurquoise2-ERlumen, the marker of ER-PM junctions GFP-MAPPER, or the Golgi marker GFP-Golgi. Cells were imaged using epifluorescence microscopy. Representative cells are shown. Colocalization values were mTurquoise2-ERlumen ($r = 0.96 \pm 0.03$, $n = 10$); GFP-MAPPER ($r = 0.94 \pm 0.02$, $n = 5$); and GFP-Golgi ($r = 0.91 \pm 0.06$, $n = 4$). **c** Schematic of ssRNb-GFP bound to RFP. **d** HeLa cells co-expressing ssRNb-GFP and either mCh-ERlumen or mCh-MAPPER were imaged using epifluorescence microscopy. Representative cells are shown. Colocalization values were: mCh-ERlumen ($r = 0.98 \pm 0.009$, $n = 9$) and mCh-MAPPER ($r = 0.93 \pm 0.07$, $n = 13$). Scale bars 10 μm (main images) and 2.5 μm (enlargements of boxed regions)

GECO1 and CMV-mito-LAR-GECO1.2 [59]; mCherry-MAPPER and mCherry-Orai1 [7].

H2B-mCh was made by transferring H2B from H2B-GFP to pmCherry-N1 (Clontech) using *KpnI/BamHI*. LAMP1-GFP was made by transferring LAMP1 from LAMP1-mCherry into pEGFP-N1 (Clontech) using *EcoRI/BamHI*. $\beta_2\text{AR}$ -mCherry was made by transferring $\beta_2\text{AR}$ from $\beta_2\text{AR}$ -mCherry to pmCherry-N1 (Clontech) using *NheI/XhoI*. $\beta_2\text{AR}$ -GFP was made by transferring GFP from pEGFP-N1 (Clontech) into $\beta_2\text{AR}$ -mCherry using *XhoI/NotI*. The mCherry-Golgi plasmid was made by

transferring mCherry from pmCherry-N1 into pEYFP-Golgi (Clontech) using *AgeI/NotI*. GFP-Golgi was made by transferring GFP from pEGFP-N1 (Clontech) into Golgi-mCherry using *AgeI/NotI*. TOM20-GFP was made by transferring EGFP from pEGFP-N1 into TOM20-mCherry using *BamHI/NotI*. TOM70-GFP-FRB was made by insertion of EGFP from pEGFP-N1 into TOM70-mCh-FRB using *AgeI/BsrGI*. SNAPf-pcDNA3.1(+) was made by transferring SNAPf from pSNAPf (New England Biolabs) to pcDNA3.1 (+) using *NheI/NotI*.

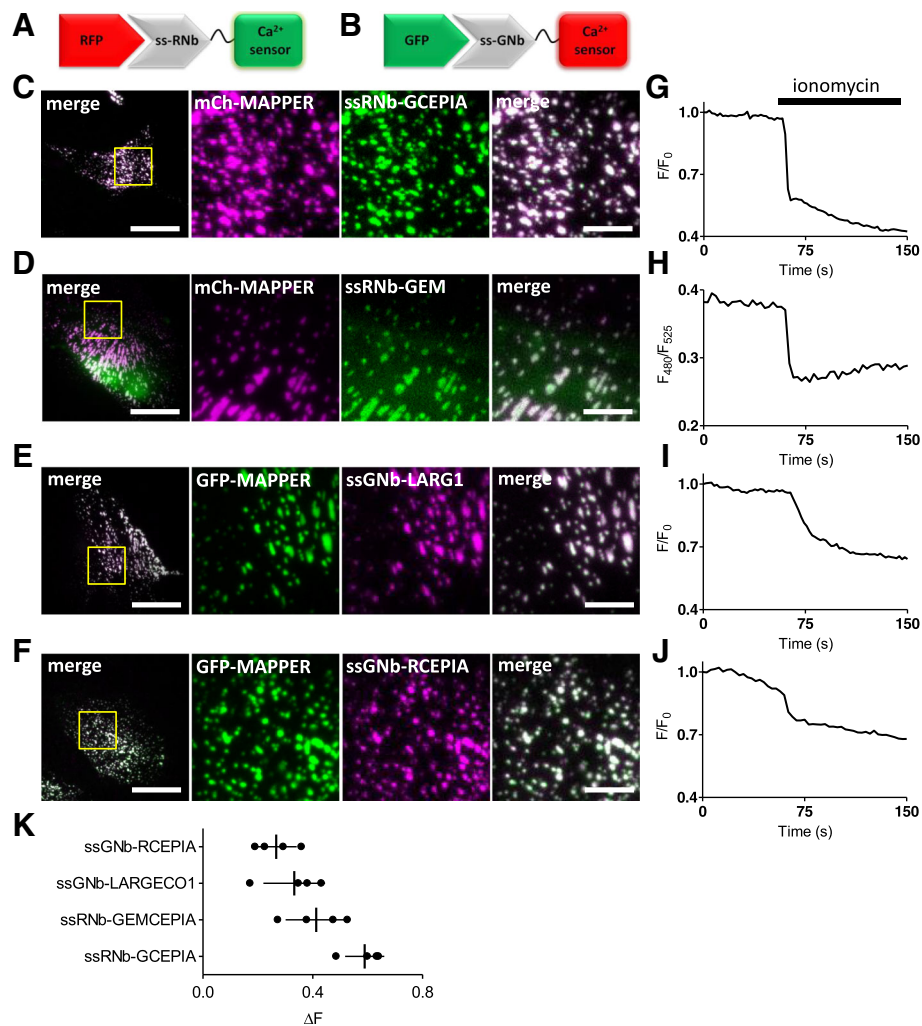


Fig. 18 Nanobody-mediated targeting of low-affinity Ca²⁺ sensors allows measurement of changes in [Ca²⁺] in an ER sub-compartment at ER-PM MCS. **a** Schematic of ssRNb-Ca²⁺ sensor bound to RFP. **b** Schematic of ssGNb-Ca²⁺ sensor bound to GFP. **c-f** HeLa cells co-expressing the indicated combinations of mCh-MAPPER, GFP-MAPPER, ssRNb-GCEPIA (ssRNb-GC), ssRNb-GEMCEPIA (ssRNb-GEM; the image is shown for the 525-nm emission channel), ssGNb-LAR-GECO1 (ssGNb-LGECO) or ssGNb-RCEPIA were imaged in Ca²⁺-free HBS using TIRFM. Yellow boxes indicate regions enlarged in subsequent images. Scale bars 10 μm (main images) and 2.5 μm (enlargements). **g-j** Timecourses of fluorescence changes recorded from cells co-expressing mCh-MAPPER and ssRNb-GCEPIA (**g**), mCh-MAPPER and ssRNb-GEMCEPIA (**h**), GFP-MAPPER and ssGNb-LAR-GECO1 (ssGNb-LARG1) (**i**) and GFP-MAPPER and ssGNb-RCEPIA (**j**) in response to emptying of intracellular Ca²⁺ stores with ionomycin (5 μM). **k** Summary results (with mean ± SD, *n* = 4 cells) show fractional decreases (ΔF) in either fluorescence or emission ratio (for ssRNb-GEM) recorded 90 s after addition of ionomycin

DNA constructs encoding GNb and RNb were synthesized as DNA Strings (ThermoFisher) and introduced by Gibson assembly (Gibson Assembly Master Mix, New England Biolabs) into pcDNA3.1(+) digested with *Bam*HI/*Eco*RI. Sequences encoding GNb and RNb are shown in Additional file 1: Figure S6. Plasmids encoding nanobody fusion constructs (Fig. 1) were constructed from the GNb and RNb plasmids using PCR, restriction digestion and ligation, or synthetic DNA Strings and Gibson assembly, and their sequences were confirmed.

GNb-mCherry was made by PCR of pmCherry-N1 using forward (ACTGGATCCATGGTGAGCAAGGGC-GAG) and reverse (GTACTCGAGCTACTTGTACAG CTCGTCCATGC) primers, followed by insertion into GNb-pcDNA3.1(+) using *Bam*HI/*Xho*I. RNb-GFP was made by PCR of pEGFP-N1 using forward (ACTGGATCCATGGTGAGCAAGGGC-GAG) and reverse (GTACTCGAGCTACTTGTACAGCTCGTCCATGC) primers, followed by insertion into RNb-pcDNA3.1(+) using *Bam*HI/*Xho*I. RNb-mCerulean-MP was made by PCR of RNb using forward (ATGCTAGCAAGCTTGCCACCATGGCTC)

and reverse (ATACCGGTGAGGATCCAGAGCCTCCGC) primers, followed by insertion into CIB1-mCerulean-MP using *NheI/AgeI*. GNB-mRFP-MP was made by PCR of GNB-FKBP with forward (TAGCTAGCGCCACCATGGCTCAGGTG) and reverse (CGACCGGTACGGACACGGTCACCTGGG) primers, followed by insertion into CIB1-mRFP1-MP using *NheI/AgeI*. GNB-SNAPf and RNB-SNAPf were made by PCR of GNB-pcDNA3.1(+) and RNB-pcDNA3.1(+) using forward (CAGCTAGCTTGGTACCGAGCTCAAGCTTGC) and reverse (ATGAATTCAGATCCCCCTCCGCCAC) primers, followed by insertion into SNAPf-pcDNA3.1 (+) using *NheI/EcoRI*. GNB-LAR-GECO1.2 was made by PCR of CMV-mito-LAR-GECO1.2 using forward (CAGGATCCATGGT-CGACTCTTACGTCGTAAGTGG) and reverse (GTAC TCGAGCTACTTCGCTGTCATCATTTGTACAAACT) primers, followed by insertion into GNB-pcDNA3.1(+) using *BamHI/XhoI*. RNB-GGECO1.2 was made by PCR of CMV-G-GECO1.2 using forward (CAGGATC-CATGGTTCGACTCATCACGTCGTAAG) and reverse (TACGATGGGCCCCTACTTCGCTGTCATCATTTG-TACAAACTCTTC) primers, followed by insertion into RNB-pcDNA3.1(+) using *BamHI/ApaI*. RNB-Perceval-HR was made by PCR of Perceval-HR with forward (AAGCGGCCGCTATGAAAAGGTTGAATCCAT-CATCAGGCC) and reverse (ATCTCGAGTCA-CAGTGCTTCCCTTGCCCTC) primers, followed by insertion into RNB-pcDNA3.1(+) using *NotI/XhoI*.

ssGNB-mCherry was made by inserting mCherry from GNB-mCherry into ssGNB-FKBP using *BamHI/NotI*. ssRNB-GFP was made by inserting GFP from RNB-GFP into ssRNB-pcDNA3.1(+) using *BamHI/NotI*. ssGNB-RCEPIA was made by transferring RCEPIA from pCMV-R-CEPIA1er to ssRNB-pcDNA3.1(+) using *BamHI/NotI*. ssGNB-LAR-GECO1 was made by transferring a DNA String encoding ssGNB into CMV-ER-LAR-GECO1 using *HindIII/BamHI*. ssRNB-GCEPIA was made by transferring GCEPIA from pCMV-G-CEPIA1er to ssRNB-pcDNA3.1(+) using *BamHI/NotI*. ssRNB-GEMCEPIA was made by transferring GEMCEPIA from pCIS-GEMCEPIA1er to ssRNB-pcDNA3.1(+) using *BamHI/NotI*.

Cell culture and transient transfection

HeLa and COS-7 cells (American Type Culture Collection) were cultured in Dulbecco's modified Eagle's medium/F-12 with GlutaMAX (ThermoFisher) supplemented with foetal bovine serum (FBS, 10%, Sigma). Cells were maintained at 37 °C in humidified air with 5% CO₂ and passaged every 3–4 days using Gibco TrypLE Express (ThermoFisher). For imaging, cells were grown on 35-mm glass-bottomed dishes (#P35G-1.0-14-C, MatTek) coated with human fibronectin (10 µg.ml⁻¹). Cells were transfected, according to the manufacturer's instructions, using TransIT-LT1 (GeneFlow) (1 µg DNA per 2.5 µl reagent). Short tandem repeat profiling

(Eurofins, Germany) was used to authenticate the identity of HeLa cells [7]. Screening confirmed that all cells were free of mycoplasma infection.

Fluorescence microscopy and analysis

Cells were washed prior to imaging at 20 °C in HEPES-buffered saline (HBS: NaCl 135 mM, KCl 5.9 mM, MgCl₂ 1.2 mM, CaCl₂ 1.5 mM, HEPES 11.6 mM, D-glucose 11.5 mM, pH 7.3). Ca²⁺-free HBS lacked CaCl₂ and contained EGTA (1 mM). For manipulations of intracellular pH, cells were imaged in modified HBS (MHBS: KCl 140 mM, MgCl₂ 1.2 mM, CaCl₂ 1.5 mM, HEPES 11.6 mM, D-glucose 11.5 mM, pH 7.2). The H⁺/K⁺ ionophore nigericin (10 µM) was added 5 min before imaging to equilibrate intracellular and extracellular pH, and the extracellular pH was then varied during imaging by exchanging the MHBS (pH 6.5 or pH 8).

Fluorescence microscopy was performed at 20 °C as described previously [7] using an inverted Olympus IX83 microscope equipped with a ×100 oil-immersion TIRF objective (numerical aperture, NA 1.49), a multi-line laser bank (425, 488, 561 and 647 nm) and an iLas2 targeted laser illumination system (Cairn, Faversham, Kent, UK). Excitation light was transmitted through either a quad dichroic beam splitter (TRF89902-QUAD) or a dichroic mirror (for 425 nm; ZT442rdc-UF2) (Chroma). Emitted light was passed through appropriate filters (Cairn Optospin; peak/bandwidth: 480/40, 525/50, 630/75 and 700/75 nm) and detected with an iXon Ultra 897 electron multiplied charge-coupled device (EMCCD) camera (512 × 512 pixels, Andor). For TIRFM, the penetration depth was 100 nm. The iLas2 illumination system was used for TIRFM and wide-field imaging. For experiments with RNB-Perceval-HR, a ×150 oil-immersion TIRF objective (NA 1.45) and a Prime 95B Scientific metal-oxide-semiconductor (CMOS) camera (512 × 512 pixels, Photometrics) were used.

For CALI and LOV2/zdk1 experiments, the 488-nm laser in the upright position delivered an output at the objective of 2.45 mW (PM100A power meter, Thor Labs, Newton, NJ, USA). For CALI, a single flash of 488-nm laser illumination (3-s duration) was applied, with 10-ms exposures to 488-nm laser immediately before and after the CALI flash to allow imaging of SNAP-Cell-fluorescein (i.e. 3.02 s total CALI flash). For LOV2/zdk1 experiments, repeated flashes of 488-nm light (1-s duration each) were used at 2-s intervals to allow imaging with 561-nm laser illumination during the intervening periods.

Before analysis, all fluorescence images were corrected for background by subtraction of fluorescence detected from a region outside the cell. Image capture and processing used MetaMorph Microscopy Automation and Image Analysis Software (Molecular Devices) and Fiji

[95]. Particle tracking used the TrackMate ImageJ plugin [96], with an estimated blob diameter of 17 pixels and a threshold of 5 pixels. Co-localization analysis used the JACoP ImageJ plugin [97]. Pearson's correlation coefficient (r) was used to quantify colocalization. We report r values only when the Costes' randomization-based colocalization value (P value = 100 after 100 iterations) confirmed the significance of the original colocalization. Where example images are shown, they are representative of at least three independent experiments (individual plates of cells from different transfections and days).

Statistics

Results are presented as mean \pm SEM for particle-tracking analyses and mean \pm SD for colocalization analyses, from n independent analyses (individual plates of cells from different transfections). Statistical comparisons used paired or unpaired Student's t tests, or analysis of variance with the Bonferroni correction used for multiple comparisons. * $P < 0.05$ was considered significant.

Additional files

Additional file 1: Figure S1. Targeting Rnb-GEMGECO Ca^{2+} sensor to RFP-tagged proteins. **Figure S2.** Targeting CALI to lysosomes with SNAP-Cell-fluorescein: cytosolic controls. **Figure S3.** Rapamycin alone does not recruit RFP-tagged or GFP-tagged proteins to mitochondria. **Figure S4.** Recruitment of proteins to native PM-mitochondria MCS using Gnb-FKBP. **Figure S5.** Inducible crosslinking of RFP-tagged and GFP-tagged proteins with Rnb-FKBP and Gnb-FRB. **Figure S6.** DNA sequences encoding the nanobodies used. (PPTX 7375 kb)

Additional file 2: Video 1. Rnb-GGECO1.2 detects changes in $[\text{Ca}^{2+}]_c$ at the surface of mitochondria expressing TOM20-mCh. The top panel shows Rnb-GGECO1.2 fluorescence (488-nm TIRFM excitation), and the bottom panel shows TOM20-mCh fluorescence (561-nm TIRFM excitation). In response to histamine (100 μM , added at 60 s), local rises in $[\text{Ca}^{2+}]_c$ were detected at the surfaces of individual mitochondria, but not in the bulk cytosol. Ionomycin (5 μM) was added at 3 min. The video was acquired at 1 Hz and is shown at 30 frames per second (fps). The clock is in mins. Relates to Fig. 3d. (MP4 75 kb)

Additional file 3: Video 2. Gnb-LARGECO1.2 detects local changes in $[\text{Ca}^{2+}]_c$ at the surface of mitochondria expressing TOM20-GFP. The video shows Gnb-LARGECO1.2 fluorescence (488-nm TIRFM excitation). Histamine (100 μM , added at 60 s) causes local rises in $[\text{Ca}^{2+}]_c$ at the OMM of individual mitochondria in the perinuclear region (cyan box in Fig. 4d), but not in peripheral regions (e.g. yellow box in Fig. 4d). Ionomycin (5 μM) was added at 3 min. The video was acquired at 1 Hz and is shown at 33 fps. The clock is in mins. Relates to Fig. 4d–f. (MP4 2807 kb)

Additional file 4: Video 3. Effect of targeted CALI on lysosomal motility. HeLa cells expressing LAMP1-mCh and Rnb-SNAPf were imaged using TIRFM and 561-nm laser illumination before (top) and after (bottom) CALI (3.02 s exposure to 488-nm epifluorescence laser illumination). The video was acquired at 0.5 Hz and is shown at 3 fps. The clock is in mins. Relates to Fig. 8. (MP4 776 kb)

Additional file 5: Video 4 Rnb-FKBP rapidly sequesters an ER integral membrane protein at the OMM. TIRFM images of HeLa cells expressing TOM70-GFP-FRB, Rnb-FKBP and mCh-Sec61 β were treated with rapamycin (100 nM, added at 60 s). The ER membrane protein, mCh-Sec61 β , is then rapidly sequestered at the OMM. The video was acquired at 0.5 Hz and shown at 33 fps. The clock is in mins. Relates to Fig. 10c, d. (MP4 551 kb)

Additional file 6: Video 5. Gnb-FKBP rapidly sequesters endogenously tagged GFP-IP $_3$ R1 at the OMM. TIRFM images show HeLa cells with endogenously GFP-tagged IP $_3$ R1 and transiently expressing TOM70-mCh-FRB and Gnb-FKBP, and then treated with rapamycin (100 nM, added at 60 s). GFP-IP $_3$ R1 is rapidly sequestered at the OMM. The video was acquired at 0.5 Hz and is shown at 33 fps. The clock is in mins. Relates to Fig. 10f and g. (MP4 2601 kb)

Additional file 7: Video 6. Gnb-FKBP rapidly sequesters GFP-CaM at the OMM. Epifluorescence microscopy images show HeLa cells transiently expressing GFP-CaM, Gnb-FKBP and TOM20-mCh-FRB, and then treated with rapamycin (100 nM, added at 30 s). GFP-CaM is rapidly sequestered at the OMM. The video was acquired at 0.5 Hz and is shown at 9 fps. The clock is in mins. Relates to Fig. 10h. (MP4 362 kb)

Additional file 8: Video 7. Rnb-FKBP recruits a PM protein to the OMM in response to rapamycin. TIRFM images of HeLa cells expressing TOM70-GFP-FRB, Rnb-FKBP and the PM protein, β_2 AR-mCh, and then exposed to rapamycin (100 nM, added at 60 s). There is a rapid translocation of β_2 AR-mCh to the OMM. The video was acquired at 0.5 Hz and is shown at 33 fps. The clock is in mins. Relates to Fig. 12b–e. (MP4 2141 kb)

Additional file 9: Video 8. Crosslinking Gnb-FKBP and Rnb-FRB with rapamycin recruits mCh-Sec61 β to TOM20-GFP in the OMM. HeLa cells expressing Gnb-FKBP, Rnb-FRB, mCh-Sec61 β and TOM20-GFP were stimulated with rapamycin (100 nM, added at 100 s). The TIRFM images show rapid recruitment of mCh-Sec61 β to the OMM. The video was acquired at 0.2 Hz and is shown at 8 fps. The clock is in mins. Relates to Fig. 16. (MP4 657 kb)

Abbreviations

$[\text{Ca}^{2+}]_c$: Cytosolic free Ca^{2+} concentration; BFP: Blue fluorescent protein; CALI: Chromophore-assisted light inactivation; CaM: Calmodulin; CFP: Cyan fluorescent protein; ER: Endoplasmic reticulum; FKBP: FK506-binding protein; FP: Fluorescent protein; FRB: FKBP-rapamycin-binding domain; GFP: Green fluorescent protein; Gnb: GFP-binding nanobody; HBS: HEPES-buffered saline; IP $_3$ R: Inositol 1,4,5-trisphosphate receptor; LAMP1: Lysosomal membrane protein 1; mCherry: Monomeric Cherry; MCS: Membrane contact site; MHBS: Modified HBS; MP: Multimerizing protein; mRFP: Monomeric red fluorescent protein; OMM: Outer mitochondrial membrane; PM: Plasma membrane; RFP: Red fluorescent protein; Rnb: RFP-binding nanobody; ROI: Region of interest; SOCE: Store-operated Ca^{2+} entry; TIRFM: Total internal reflection fluorescence microscopy; YFP: Yellow fluorescent protein

Acknowledgements

Not applicable.

Funding

This work was supported by the Biotechnology and Biological Sciences Research Council UK (grant number BB/P005330/1) and a Wellcome Trust Senior Investigator Award (grant number 101844).

Availability of data and materials

All plasmids and data generated or analysed during this study are included in this published article and its supplementary information files. Plasmids are available from the corresponding authors on request and from Addgene.

Authors' contributions

DLP and CWT conceived the work. DLP conducted all the experiments and analysis. DLP and CWT interpreted the data and wrote the manuscript. DLP and CWT read and approved the final manuscript.

Ethics approval and consent to participate

Not applicable

Competing interests

The authors declare that they have no competing interests.

Publisher's Note

Springer Nature remains neutral with regard to jurisdictional claims in published maps and institutional affiliations.

Received: 6 February 2019 Accepted: 2 May 2019

Published online: 23 May 2019

References

- Clift D, McEwan WA, Labzin LI, Konieczny V, Mogessie B, James LC, et al. A method for the acute and rapid degradation of endogenous proteins. *Cell*. 2018;171:1692–706 e18.
- Helma J, Cardoso MC, Muyldermans S, Leonhardt H. Nanobodies and recombinant binders in cell biology. *J Cell Biol*. 2015;209:633–44.
- Shaner NC, Steinbach PA, Tsien RY. A guide to choosing fluorescent proteins. *Nat Methods*. 2005;2:905–9.
- Rodriguez EA, Campbell RE, Lin JY, Lin MZ, Miyawaki A, Palmer AE, et al. The growing and glowing toolbox of fluorescent and photoactive proteins. *Trends Biochem Sci*. 2017;42:111–29.
- Leonetti MD, Sekine S, Kamiyama D, Weissman JS, Huang B. A scalable strategy for high-throughput GFP tagging of endogenous human proteins. *Proc Natl Acad Sci U S A*. 2016;113:E3501–8.
- Stewart-Ornstein J, Lahav G. Dynamics of CDKN1A in single cells defined by an endogenous fluorescent tagging toolkit. *Cell Rep*. 2016;14:1800–11.
- Thillaiappan NB, Chavda AP, Tovey SC, Prole DL, Taylor CW. Ca²⁺ signals initiate at immobile IP₃ receptors adjacent to ER-plasma membrane junctions. *Nat Commun*. 2017;8:1505.
- Zhang J. The colorful journey of green fluorescent protein. *ACS Chem Biol*. 2009;4:85–8.
- Stadler C, Rexhepaj E, Singan VR, Murphy RF, Pepperkok R, Uhlen M, et al. Immunofluorescence and fluorescent-protein tagging show high correlation for protein localization in mammalian cells. *Nat Methods*. 2013;10:315–23.
- Hein MY, Hubner NC, Poser I, Cox J, Nagaraj N, Toyoda Y, et al. A human interactome in three quantitative dimensions organized by stoichiometries and abundances. *Cell*. 2015;163:712–23.
- Nagarkar-Jaiswal S, Lee PT, Campbell ME, Chen K, Anguiano-Zarate S, Gutierrez MC, et al. A library of MiMICs allows tagging of genes and reversible, spatial and temporal knockdown of proteins in *Drosophila*. *eLife*. 2015;4:e05338.
- Huh WK, Falvo JV, Gerke LC, Carroll AS, Howson RW, Weissman JS, et al. Global analysis of protein localization in budding yeast. *Nature*. 2003;425:686–91.
- Hayashi A, Ding DQ, Tsutsumi C, Chikashige Y, Masuda H, Haraguchi T, et al. Localization of gene products using a chromosomally tagged GFP-fusion library in the fission yeast *Schizosaccharomyces pombe*. *Genes Cells*. 2009;14:217–25.
- Yofe I, Weill U, Meurer M, Churtzman S, Zalckvar E, Goldman O, et al. One library to make them all: streamlining the creation of yeast libraries via a SWAp-tag strategy. *Nat Methods*. 2016;13:371–8.
- Koroleva OA, Tomlinson ML, Leader D, Shaw P, Doonan JH. High-throughput protein localization in *Arabidopsis* using *Agrobacterium*-mediated transient expression of GFP-ORF fusions. *Plant J*. 2005;41:162–74.
- Tian GW, Mohanty A, Chary SN, Li S, Paap B, Drakakaki G, et al. High-throughput fluorescent tagging of full-length *Arabidopsis* gene products in planta. *Plant Physiol*. 2004;135:25–38.
- Kitagawa M, Ara T, Arifuzzaman M, Ioka-Nakamichi T, Inamoto E, Toyonaga H, et al. Complete set of ORF clones of *Escherichia coli* ASKA library (a complete set of *E. coli* K-12 ORF archive): unique resources for biological research. *DNA Res*. 2005;12:291–9.
- Eason MG, Damry AM, Chica RA. Structure-guided rational design of red fluorescent proteins: towards designer genetically-encoded fluorophores. *Curr Opin Struct Biol*. 2017;45:91–9.
- Harikumar A, Edupuganti RR, Sorek M, Azad GK, Markoulaki S, Sehnalova P, et al. An endogenously tagged fluorescent fusion protein library in mouse embryonic stem cells. *Stem Cell Rep*. 2017;9:1304–14.
- Pollithy A, Romer T, Lang C, Muller FD, Helma J, Leonhardt H, et al. Magnetosome expression of functional camelid antibody fragments (nanobodies) in *Magnetospirillum gryphiswaldense*. *Appl Environ Microbiol*. 2011;77:6165–71.
- Fridy PC, Li Y, Keegan S, Thompson MK, Nudelman I, Scheid JF, et al. A robust pipeline for rapid production of versatile nanobody repertoires. *Nat Methods*. 2014;11:1253–60.
- Rothbauer U, Zolghadr K, Muyldermans S, Schepers A, Cardoso MC, Leonhardt H. A versatile nanotrapp for biochemical and functional studies with fluorescent fusion proteins. *Mol Cell Proteomics*. 2008;7:282–9.
- Kanner SA, Morgenstern T, Colecraft HM. Sculpting ion channel functional expression with engineered ubiquitin ligases. *eLife*. 2017;6:e29744.
- Causinus E, Kanca O, Affolter M. Fluorescent fusion protein knockout mediated by anti-GFP nanobody. *Nat Struct Mol Biol*. 2011;19:117–21.
- Borg S, Popp F, Hofmann J, Leonhardt H, Rothbauer U, Schuler D. An intracellular nanotrapp redirects proteins and organelles in live bacteria. *MBio*. 2015;6:e02117.
- Liu TK, Hsieh PY, Zhuang YD, Hsia CY, Huang CL, Lai HP, et al. A rapid SNAP-tag fluorogenic probe based on an environment-sensitive fluorophore for no-wash live cell imaging. *ACS Chem Biol*. 2014;9:2359–65.
- Filadi R, Pozzan T. Generation and functions of second messengers microdomains. *Cell Calcium*. 2015;58:405–14.
- Ludwig FT, Schwab A, Stock C. The Na⁺/H⁺–exchanger (NHE1) generates pH nanodomains at focal adhesions. *J Cell Physiol*. 2012;228:1351–8.
- Schlattner U, Klaus A, Ramirez Rios S, Guzun R, Kay L, Tokarska-Schlattner M. Cellular compartmentation of energy metabolism: creatine kinase microcompartments and recruitment of B-type creatine kinase to specific subcellular sites. *Amino Acids*. 2016;48:1751–74.
- Zhao Y, Araki S, Wu J, Teramoto T, Chang YF, Nakano M, et al. An expanded palette of genetically encoded Ca²⁺ indicators. *Science*. 2011;333:1888–91.
- Sankaranarayanan S, De Angelis D, Rothman JE, Ryan TA. The use of pHluorins for optical measurements of presynaptic activity. *Biophys J*. 2000;79:2199–208.
- Shen Y, Rosendale M, Campbell RE, Perrais D. pHuji, a pH-sensitive red fluorescent protein for imaging of exo- and endocytosis. *J Cell Biol*. 2014;207:419–32.
- Tantama M, Martinez-Francois JR, Mongeon R, Yellen G. Imaging energy status in live cells with a fluorescent biosensor of the intracellular ATP-to-ADP ratio. *Nat Commun*. 2013;4:2550.
- Atakpa P, Thillaiappan NB, Mataragka S, Prole DL, Taylor CW. IP₃ receptors preferentially associate with ER-lysosome contact sites and selectively deliver Ca²⁺ to lysosomes. *Cell Rep*. 2018;25:3180–93.
- Mammucari C, Raffaello A, Vecellio Reane D, Gherardi G, De Mario A, Rizzuto R. Mitochondrial calcium uptake in organ physiology: from molecular mechanism to animal models. *Pflugers Arch*. 2018;470:1165–79.
- Wang X, Schwarz TL. The mechanism of Ca²⁺–dependent regulation of kinesin-mediated mitochondrial motility. *Cell*. 2009;136:163–74.
- Hajnóczky G, Robb-Gaspers LD, Seitz MB, Thomas AP. Decoding cytosolic calcium oscillations in the mitochondria. *Cell*. 1995;82:415–24.
- Giacomello M, Drago I, Bortolozzi M, Scorsetto M, Gianella A, Pizzo P, et al. Ca²⁺ hot spots on the mitochondrial surface are generated by Ca²⁺ mobilization from stores, but not by activation of store-operated Ca²⁺ channels. *Mol Cell*. 2010;38:280–90.
- Cole NB. Site-specific protein labeling with SNAP-tags. *Curr Prot Prot Sci*. 2013;73:30.1.1–30.1.16.
- Ries J, Kaplan C, Platonova E, Eghlidi H, Ewers H. A simple, versatile method for GFP-based super-resolution microscopy via nanobodies. *Nat Methods*. 2012;9:582–4.
- Bodor DL, Rodriguez MG, Moreno N, Jansen LE. Analysis of protein turnover by quantitative SNAP-based pulse-chase imaging. *Curr Prot Cell Biol*. 2012;55:8.1–8.8.34.
- Sano Y, Watanabe W, Matsunaga S. Chromophore-assisted laser inactivation - towards a spatiotemporal-functional analysis of proteins, and the ablation of chromatin, organelle and cell function. *J Cell Sci*. 2014;127:1621–9.
- Bonifacino JS, Neeffes J. Moving and positioning the endolysosomal system. *Curr Opin Cell Biol*. 2017;47:1–8.
- Lee S, Park H, Kyung T, Kim NY, Kim J, et al. Reversible protein inactivation by optogenetic trapping in cells. *Nat Methods*. 2014;11:633–6.
- Robinson MS, Sahlender DA, Foster SD. Rapid inactivation of proteins by rapamycin-induced rerouting to mitochondria. *Dev Cell*. 2010;18:324–31.
- Wang H, Vilela M, Winkler A, Tarnawski M, Schlichting I, Yumerefendi H, et al. LOVTRAP: an optogenetic system for photoinduced protein dissociation. *Nat Methods*. 2016;13:755–8.
- Csordas G, Weaver D, Hajnoczky G. Endoplasmic reticular-mitochondrial contactology: structure and signaling functions. *Trends Cell Biol*. 2018;28:523–40.
- Csordas G, Varnai P, Golenar T, Roy S, Purkins G, Schneider TG, et al. Imaging interorganelle contacts and local calcium dynamics at the ER-mitochondrial interface. *Mol Cell*. 2010;39:121–32.
- Tepikin AV. Mitochondrial junctions with cellular organelles: Ca²⁺ signalling perspective. *Pflugers Arch*. 2018;470:1181–92.
- Kennedy HJ, Pouli AE, Ainscow EK, Jouaville LS, Rizzuto R, Rutter GA. Glucose generates sub-plasma membrane ATP microdomains in single islet beta-cells. Potential role for strategically located mitochondria. *J Biol Chem*. 1999;274:13281–91.

51. Quintana A, Pasche M, Junker C, Al-Ansary D, Rieger H, Kummerow C, et al. Calcium microdomains at the immunological synapse: how ORAI channels, mitochondria and calcium pumps generate local calcium signals for efficient T-cell activation. *EMBO J*. 2011;30:3895–912.
52. Frieden M, Arnaudeau S, Castelbou C, Demaurex N. Subplasmalemmal mitochondria modulate the activity of plasma membrane Ca^{2+} -ATPases. *J Biol Chem*. 2005;280:43198–208.
53. Balla T. Ca^{2+} and lipid signals hold hands at endoplasmic reticulum-plasma membrane contact sites. *J Physiol*. 2017;596:2709–16.
54. Prakriya M, Lewis RS. Store-operated calcium channels. *Physiol Rev*. 2015;95:1383–436.
55. Chang CL, Hsieh TS, Yang TT, Rothberg KG, Azizoglu DB, Volk E, et al. Feedback regulation of receptor-induced Ca^{2+} signaling mediated by E-Syt1 and Nir2 at endoplasmic reticulum-plasma membrane junctions. *Cell Rep*. 2013;5:813–25.
56. Simmen T, Tagaya M. Organelle communication at membrane contact sites (MCS): from curiosity to center stage in cell biology and biomedical research. *Adv Exp Med Biol*. 2017;997:1–12.
57. Wong YC, Ysselstein D, Krainc D. Mitochondria-lysosome contacts regulate mitochondrial fission via RAB7 GTP hydrolysis. *Nature*. 2017;554:382–6.
58. Torres S, Balboa E, Zanlungo S, Enrich C, Garcia-Ruiz C, Fernandez-Checa JC. Lysosomal and mitochondrial liaisons in Niemann-Pick disease. *Front Physiol*. 2017;8:982.
59. Wu J, Prole DL, Shen Y, Lin Z, Gnanasekaran A, Liu Y, et al. Red fluorescent genetically encoded Ca^{2+} indicators for use in mitochondria and endoplasmic reticulum. *Biochem J*. 2014;464:13–22.
60. Suzuki J, Kanemaru K, Ishii K, Ohkura M, Okubo Y, Iino M. Imaging intracellular Ca^{2+} at subcellular resolution using CEPIA. *Nat Commun*. 2014;5:4153.
61. Suzuki J, Kanemaru K, Iino M. Genetically encoded fluorescent indicators for organelle calcium imaging. *Biophys J*. 2016;111:1119–31.
62. Hirabayashi Y, Kwon SK, Paek H, Pernice WM, Paul MA, Lee J, et al. ER-mitochondria tethering by PDZD8 regulates Ca^{2+} dynamics in mammalian neurons. *Science*. 2017;358:623–30.
63. Konieczny V, Tovey SC, Mataragka S, Prole DL, Taylor CW. Cyclic AMP recruits a discrete intracellular Ca^{2+} store by unmasking hypersensitive IP_3 receptors. *Cell Rep*. 2017;18:711–22.
64. Rodriguez-Prados M, Rojo-Ruiz J, Aulestia FJ, Garcia-Sancho J, Alonso MT. A new low- Ca^{2+} affinity GAP indicator to monitor high Ca^{2+} in organelles by luminescence. *Cell Calcium*. 2015;58:558–64.
65. Konieczny V, Keebler MV, Taylor CW. Spatial organization of intracellular Ca^{2+} signals. *Semin Cell Dev Biol*. 2012;23:172–80.
66. Langeberg LK, Scott JD. Signalling scaffolds and local organization of cellular behaviour. *Nat Rev Mol Cell Biol*. 2015;16:232–44.
67. Ariotti N, Rae J, Giles N, Martel N, Sierrecki E, Gambin Y, et al. Ultrastructural localisation of protein interactions using conditionally stable nanobodies. *PLoS Biol*. 2018;16:e2005473.
68. Rost BR, Schneider-Warme F, Schmitz D, Hegemann P. Optogenetic tools for subcellular applications in neuroscience. *Neuron*. 2017;96:572–603.
69. Ruggiu AA, Bannwarth M, Johnsson K. Fura-2FF-based calcium indicator for protein labeling. *Org Biomol Chem*. 2010;8:3398–401.
70. Kamiya M, Johnsson K. Localizable and highly sensitive calcium indicator based on a BODIPY fluorophore. *Anal Chem*. 2010;82:6472–9.
71. Bannwarth M, Correa IR, Sztrétye M, Pouvreau S, Fellay C, Aebischer A, et al. Indo-1 derivatives for local calcium sensing. *ACS Chem Biol*. 2009;4:179–90.
72. Wang C, Song X, Xiao Y. SNAP-tag-based subcellular protein labeling and fluorescent imaging with naphthalimides. *ChemBioChem*. 2017;18:1762–9.
73. Abo M, Minakami R, Miyano K, Kamiya M, Nagano T, Urano Y, et al. Visualization of phagosomal hydrogen peroxide production by a novel fluorescent probe that is localized via SNAP-tag labeling. *Anal Chem*. 2014;86:5983–90.
74. Zimmermann M, Cal R, Janett E, Hoffmann V, Bochet CG, Constable E, et al. Cell-permeant and photocleavable chemical inducer of dimerization. *Angew Chem Int Ed Engl*. 2014;53:4717–20.
75. Feng S, Laketa V, Stein F, Rutkowska A, MacNamara A, Depner S, et al. A rapidly reversible chemical dimerizer system to study lipid signaling in living cells. *Angew Chem Int Ed Engl*. 2014;53:6720–3.
76. Putyrski M, Schultz C. Protein translocation as a tool: the current rapamycin story. *FEBS Lett*. 2012;586:2097–105.
77. Marschall AL, Dubel S, Boldicke T. Specific in vivo knockdown of protein function by intrabodies. *MAbs*. 2015;7:1010–35.
78. Michelangeli F, Ogunbayo OA, Wootton LL. A plethora of interacting organellar Ca^{2+} stores. *Curr Opin Cell Biol*. 2005;17:135–40.
79. Wong AK, Capitanio P, Lissandron V, Bortolozzi M, Pozzan T, Pizzo P. Heterogeneity of Ca^{2+} handling among and within Golgi compartments. *J Mol Cell Biol*. 2013;5:266–76.
80. Crevenna AH, Blank B, Maiser A, Emin D, Prescher J, Beck G, et al. Secretory cargo sorting by Ca^{2+} -dependent Cab45 oligomerization at the trans-Golgi network. *J Cell Biol*. 2016;213:305–14.
81. Appenzeller C, Andersson H, Kappeler F, Hauri HP. The lectin ERGIC-53 is a cargo transport receptor for glycoproteins. *Nat Cell Biol*. 1999;1:330–4.
82. Mitchell KJ, Pinton P, Varadi A, Tacchetti C, Ainscow EK, Pozzan T, et al. Dense core secretory vesicles revealed as a dynamic Ca^{2+} store in neuroendocrine cells with a vesicle-associated membrane protein aequorin indicator. *J Cell Biol*. 2001;155:41–51.
83. Mundorf ML, Troyer KP, Hochstetler SE, Near JA, Wightman RM. Vesicular Ca^{2+} participates in the catalysis of exocytosis. *J Biol Chem*. 2000;275:9136–42.
84. Harmansa S, Affolter M. Protein binders and their applications in developmental biology. *Development*. 2018;145:dev148874.
85. Tiede C, Bedford R, Heseltine SJ, Smith G, Wijetunga I, Ross R, et al. Affimer proteins are versatile and renewable affinity reagents. *eLife*. 2017;6:e24903.
86. Sha F, Salzman G, Gupta A, Koide S. Monoclonal antibodies and other synthetic binding proteins for expanding protein science. *Protein Sci*. 2017;26:910–24.
87. Wozniak MJ, Bola B, Brownhill K, Yang YC, Levakova V, Allan VJ. Role of kinesin-1 and cytoplasmic dynein in endoplasmic reticulum movement in VERO cells. *J Cell Sci*. 2009;122:1979–89.
88. Lopez Sanjurjo CI, Tovey SC, Prole DL, Taylor CW. Lysosomes shape $\text{Ins}(1,4,5)\text{P}_3$ -evoked Ca^{2+} signals by selectively sequestering Ca^{2+} released from the endoplasmic reticulum. *J Cell Sci*. 2013;126:289–300.
89. Brailoiu E, Churamani D, Cai X, Schrlau MG, Brailoiu GC, Gao X, et al. Essential requirement for two-pore channel 1 in NAADP-mediated calcium signaling. *J Cell Biol*. 2009;186:201–19.
90. Kanda T, Sullivan KF, Wahl GM. Histone-GFP fusion protein enables sensitive analysis of chromosome dynamics in living mammalian cells. *Curr Biol*. 1998;8:377–85.
91. English AR, Voeltz GK. Rab10 GTPase regulates ER dynamics and morphology. *Nat Cell Biol*. 2013;15:169–78.
92. Cheeseman LP, Harry EF, McAinsh AD, Prior IA, Royle SJ. Specific removal of TACC3-ch-TOG-clathrin at metaphase deregulates kinetochore fiber tension. *J Cell Sci*. 2013;126:2102–13.
93. Goedhart J, von Stetten D, Noirclicr-Savoye M, Lelimosin M, Joosen L, Hink MA, et al. Structure-guided evolution of cyan fluorescent proteins towards a quantum yield of 93%. *Nat Commun*. 2012;3:751.
94. Violin JD, Ren XR, Lefkowitz RJ. G-protein-coupled receptor specificity for β -arrestin recruitment to the β_2 -adrenergic receptor revealed by fluorescence resonance energy transfer. *J Biol Chem*. 2006;281:20577–88.
95. Schindelin J, Arganda-Carreras I, Frise E, Kaynig V, Longair M, Pietzsch T, et al. Fiji: an open-source platform for biological-image analysis. *Nat Methods*. 2012;9:676–82.
96. Jaqaman K, Loerke D, Mettlen M, Kuwata H, Grinstein S, Schmid SL, et al. Robust single-particle tracking in live-cell time-lapse sequences. *Nat Methods*. 2008;5:695–702.
97. Bolte S, Cordelières FP. A guided tour into subcellular colocalization analysis in light microscopy. *J Microsc*. 2006;224:213–32.

Ready to submit your research? Choose BMC and benefit from:

- fast, convenient online submission
- thorough peer review by experienced researchers in your field
- rapid publication on acceptance
- support for research data, including large and complex data types
- gold Open Access which fosters wider collaboration and increased citations
- maximum visibility for your research: over 100M website views per year

At BMC, research is always in progress.

Learn more biomedcentral.com/submissions

